Czech Technical University in Prague
Faculty of Nuclear Sciences and Physical Engineering

Department of Physics

COMPASS Tokamak Experiments Support by Simulations

DIPLOMA THESIS

Author: Bc. Adam Seman
Supervisor: Ing. Jakub Urban, Ph.D.
Submitted in: January 2017

Insert ASSIGNMENT here.

Prohlášení

Prohlašuji, že jsem svou diplomovou práci vypracoval samostatně a použil jsem pouze podklady (literaturu, projekty, SW atd.) uvedené v přiloženém seznamu.

Nemám závažný důvod proti použití tohoto školního díla ve smyslu § 60 Zákona č.121/2000 Sb., o právu autorském, o právech souvisejících s právem autorským a o změně některých zákonů (autorský zákon).

V Praze dne .....

.....
Bc. Adam Seman

Poďakovanie

Poďakovanie by som chcel venovať predovšetkým môjmu školiteľovi, Ing. Jakubovi Urbanovi, PhD. za všetok ochotne strávený čas a podnetné rady, vďaka ktorým mohla táto práca vzniknúť. V neposlednej rade by som sa chcel poďakovať rodičom, ktorí ma podporovali a umožňovali mi pracovať v kreatívnom pracovnom prostredí. Špeciálne poďakovanie patrí Klaudii Málekovej, ktorá mi bola veľkou oporou pri tvorení diplomovej práce.

Bc. Adam Seman

Název práce:
Podpora experimentů v tokamaku COMPASS pomocí simulací

Autor: Bc. Adam Seman

Obor: Fyzika a technika termojaderné fúze

Druh práce: Diplomová práce

Vedoucí práce: Ing. Jakub Urban, Ph.D.
Institute of Plasma Physics AS CR, v.v.i., Assoc EUROATOM-IPP.CR

Konzultant: -
-

Abstrakt: Táto práca sa zaoberá podporou experimentov na tokamaku COMPASS pomocou simulacií. Prvá kapitola tejto práce sa zaoberá základnou teóriou riadenej termojadrovej fúzie a definícii jej fundamentálnych pojmov. Druhá kapitola pojednáva fyzikálne a technické aspekty dodatočného ohrevu vysokoteplotnej plazmy pomocou injekcie neutrálnych zväzkov – NBI. Podpora pomocou počítačových simulácií bola vykonaná predovšetkým na experimentoch s NBI, preto bola tejto tematike venovaná separátna kapitola. Tretia kapitola sa zaoberala počítačovými simuláciami NBI v tokamakovej plazme a ich porovnaniam. V tejto kapitole sa popisuje základný princíp a rozdiely medzi simulačnými kódmi z európskej platformy pre tokamakové modelovanie (BBNBI a RISK) a transportným simulačným kódom METIS. V rámci tejto kapitoly sa taktiež popisuje vyvijaný rýchly zjednodušený kód pre simuláciu ionizácie neutrálneho zväzku. Posledná kapitola je venovaná aplikacii spomínaných simulácií pre podporu experimentov na tokamaku COMPASS. Výsledkom simulácií sú informácie o stratových procesoch NBI a náročne merateľných veličinách ako ionizovaný výkon z NBI, profily a frakcie výkonu NBI prenesené na elektróny a ióny v plazme a distribučná funkcia iónov.

Klíčová slova: Termojadrová fúzia, Plazma, Tokamak, Simulácia, NBI

Title:
COMPASS Tokamak Experiments Support by Simulations

Author: Bc. Adam Seman

Abstract: This thesis is dedicated to COMPASS tokamak experiments support by simulations. The first chapter is devoted to basic theory of controlled thermonuclear fusion and definition of its fundamental terms. The second chapter is focused on physical and technical aspect of the additional heating of high-temperature plasma by neutral beam injection – NBI. Support by computer simulations has been performed mainly on experiments with NBI, therefore has been devoted to this subject a separate chapter. The third chapter was concerned with computer simulations of NBI in tokamak plasma and their comparisons. In this chapter is described basic principle and differences between simulation codes from European platform for tokamak modelling (BBNBI and RISK) and transport simulation code METIS. In this chapter is also described developed fast simplified code for simulation of neutral beam ionization. The last chapter is dedicated to application of mentioned simulations for COMPASS tokamak experiments support. The result of simulations is information about the loss processes of NBI and difficultly measurable quantities as the NBI ionized power, the profiles and the fractions of NBI power transferred to plasma electrons and ions and the ion distribution function.

Key words: Thermonuclear fusion, Plasma, Tokamak, Simulation, NBI

Contents

Chapter 1

Introduction

One of the most relevant and crucial topics of these days is the solution of energy resources problem and the related environmental questions. Word energy consumption increases with an exponential tendency and this effect is accompanied by many environmental complications such as increase of carbon dioxide content, atmosphere pollution and the last but not least greenhouse effect. What is worse, in parallel with this increasing tendency of the energy consumption, energy supplies are limited by fossil and nuclear fuel sources. For this reason, a source of energy, which is environmentally clean and hardly exhaustible, is urgently needed.

Renewable energy resources are one of the possible solutions of this problem, but they are not able to fully supply current energy needs. The other solution comes with the fission reactors of higher generations that would consume the current nuclear waste. Besides these solutions is one of the most perspective ways generation of energy by a nuclear fusion.

Nuclear fusion is a process of merging lighter nuclei into a heavier nucleus of high nuclear stability. This effect enables us to produce energy according to Albert Einstein special theory of relativity. The problem of this concept is that nuclei are repelling themselves by an effect of Coulomb repulsion, thus the energy of the merging nuclei has to be high enough to break the barrier of Coulomb repulsion. It has been found through the decades that the most appropriate elements for nuclear fusion are heavier isotopes of hydrogen due to their physical properties and availability on Earth.

The state of matter at the energies required for fusing nuclei is called high-temperature plasma. The temperatures of this state of matter are so high that any material is not sufficient as a container, which would confine the high-temperature plasma. On the other hand, plasma is an ionized gas or in other words, plasma consists of charged particles, which could be influenced by external electromagnetic fields. Thus a special configuration of electromagnetic field could be an appropriate container for high-temperature plasma. One of the most successful approaches to the plasma confinement by the electromagnetic fields is called "tokamak".

Now we know that the high-temperature plasma could be confined by the appropriate configuration of electromagnetic fields, but there is still a question how we are able to heat the plasma to temperatures high enough to fuse the hydrogen nuclei. One of the possible ways of heating the plasma is called Ohmic heating. The principle of this heating method is based on creation of electric current inside the plasma of certain resistivity and due to collision between plasma particles is the plasma heated up by Joule's heat release. A problem of

this concept is that the plasma resistivity decreases with increasing temperature and this heating method is ineffective to heat the plasma to the fusion temperatures. Therefore, another heating method is needed which would be appropriate to heat the plasma to these temperatures.

A simple principle of the plasma heating is injection of fast energetic particles inside the plasma. These fast particles are exposed to multiple Coulomb collisions with plasma particles, transferring their kinetic energy to the plasma particles kinetic energy. The resultant effect is an increase of the plasma temperature.

A problem of this concept is that the injected particles (usually ions) cannot be charged because as the electromagnetic fields confine charged plasma particles inside a certain volume, they do not allow them to penetrate inside the plasma. Therefore the fast particles have to be neutralized before they reach the plasma. The neutralized particles are not influenced by the electromagnetic fields and freely enters the plasma where are ionized. This heating method is called neutral beam injection - NBI.

Neutral beam injection is a commonly used heating method on tokamaks worldwide. Besides heating the plasma is this method also used for a generation of the electric current and a fuel delivery inside the tokamak plasma. This thesis is dedicated to tokamak experiments support by simulations focused on effects of NBI. The main focus of this thesis is on the ionization processes of NBI and the resultant plasma heating effects.

The experiments support has been made on the tokamak COMPASS, the biggest tokamak of Czech Republic situated at Institute of Plasma Physics of the CAS. Tokamak COMPASS is equipped with two neutral beam injectors, each of 300kW power and 40keV ion.

Simulation codes from the European integrated modeling platform have been used with an aim of the COMPASS tokamak experiments support. Also, has been made a fast simplified ionization model of NBI inside the tokamak COMPASS plasma. All of the acquired information and data from the simulations should help to the scientific progress of tokamak COMPASS.

Chapter 2

Physical and technological basis

This chapter is going to be dedicated to the basic physical background for exact and well-defined term definition, which is necessarily needed for purposes of this thesis. We are about to define terminology of nuclear fusion including nuclear processes, basic plasma physics, movement of particles in electromagnetic fields and subsequently the most successful approach to nuclear fusion - Tokamak.

2.1 Nuclear processes

According to Albert Einstein's mass-energy equivalence equation, mankind noticed progress not just in the field of natural knowledge, but also in the field of applied research.

$$E = mc^2 \tag{2.1}$$

Equivalence equation states that energy and mass are mutually chained quantities. We can illustrate the understanding of this equality principle on a simple example. If we make an assumption that atomic nucleus consists of protons and neutrons (nucleons), we are able to determine the mass of an atomic nucleus just by a sum of each nucleon masses of the nucleus. Despite this totally logical approach, we will not get the proper value of nucleus mass. The sum of each nucleon masses of the atomic nucleus and real atomic mass are different. This mass difference and actually energy difference is equal to the binding energy of nucleus needed to split nucleus to separate nucleons.

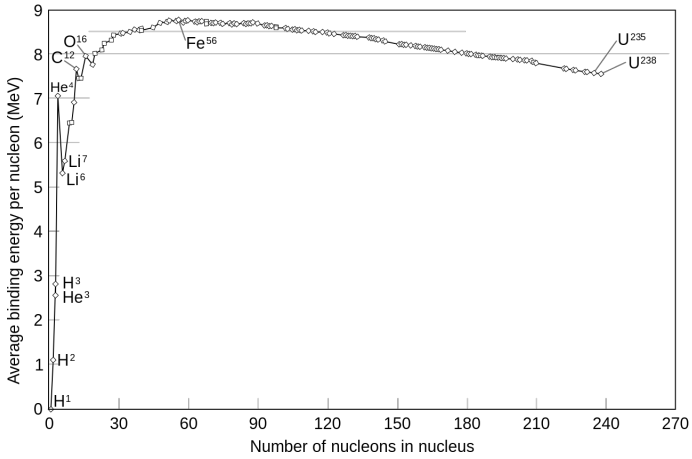

Figure 2.1: Average binding energy per nucleon in nucleus

Binding energy is the term that allows us hypothetically to create new elements from other elements, with exothermic or endothermic reaction process. Exothermic reaction process is an appropriate phenomenon for energy production for the consumer society. The rationale of energy production using nuclear processes is shown in Fig. 2.1 of average binding energy per nucleon dependent on an atomic number.

According to this dependency is obvious that we can produce energy by two nuclear processes. The first approach is nuclear fission, where the high atomic number nuclei are split into nuclei with a lower atomic number. The second principle is based on merging nuclei of low atomic number to a heavier nucleus of a high nuclear stability. This second principle is called nuclear fusion, and from now we are going to call this phenomenon just fusion.

There are multiple fusion reactions but for our purposes is relevant fusion of hydrogen isotopes (deuterium and tritium)(2.2) [1, 2], due to its high efficiency. Centre of our interest is oriented to reaction (2.2a), which released energy is transferred to kinetic energy of products - alpha particle and neutron. The kinetic energy of products is given in the brackets next to each product.

$$ {}^{2}_{1}D + {}^{3}_{1}T \quad \longrightarrow \quad {}^{4}_{2}He(3.5MeV) \quad + \quad {}^{1}_{0}n(14.1MeV) \tag{2.2a} $$

$$ {}^{2}_{1}D + {}^{2}_{1}D \quad \longrightarrow \quad {}^{3}_{2}He(0.87MeV) \quad + \quad {}^{1}_{0}n(2.45MeV) \tag{2.2b} $$

$$ {}^{2}_{1}D + {}^{2}_{1}D \quad \longrightarrow \quad {}^{3}_{1}T(1.01MeV) \quad + \quad {}^{1}_{1}p(3.02MeV) \tag{2.2c} $$

$$ {}^{2}_{1}D + {}^{3}_{2}He \quad \longrightarrow \quad {}^{4}_{2}He(3.67MeV) \quad + \quad {}^{1}_{1}p(14.7MeV) \tag{2.2d} $$

2.1.1 Cross section

Obviously, if we start to discuss nuclear processes, is usable to define quantity, which evaluates the effectiveness how colliding particles react and this quantity is called cross section. To be more specific, let us consider a uniform beam of particles with velocity v, interacting with a target containing particles at rest. The cross-section $\sigma(v)$ is defined as the number of reactions per target nucleus per unit time when the target is hit by a unit flux of projectile particles, that is, by one particle per unit target area per unit time.

Let us discuss cross section for fusion reactions. First approximation from the sight of classical physics gives us an unrealistic model of how nuclei fuse. To fuse nuclei, with respect to classical physics, is needed the kinetic energy of positively charged colliding nuclei to break Coulomb barrier until the strong interaction of nuclei starts to manifest itself. This model gives us the energy to break Coulomb for reaction (2.2a) around hundred keV.

Of course, with nuclear reactions we need to involve the effect of quantum tunneling into this model, and also define the cross section of fusion reactions with this effect included. We can define the cross section as multiplication of three coefficients (2.3a) – geometrical cross

section (2.3b), transparency barrier (2.3c), probability that nuclei come into contact fuse R [2].

$$\sigma = \sigma_{geom} \times T \times R \tag{2.3a}$$

$$\sigma_{geom} \approx \left(\frac{h}{2\pi m_r v}\right)^2 \approx \frac{1}{\epsilon} \tag{2.3b}$$

$$T \approx T_G = \exp\Big(-\sqrt{\frac{\epsilon_G}{\epsilon}}\Big), \quad \epsilon_G = 986.1(Z_1 Z_2)^2 A_r keV \tag{2.3c}$$

The geometrical cross section we can express in term of square de-Broglie wavelength, where h is Planck's constant, m_r is reduced the mass of nuclei system and v is the relative velocity of colliding nuclei. Transparency barrier is well approximated with expression (2.3c), where ϵ_G is Gamow's factor. In Gamow's factor, there are Z_1 and Z_2 as atomic numbers of colliding nuclei and A_r is a reduced mass of system divided by proton mass.

Variation of the R factor is small in comparison with strong varying Gamow's factor in transparency barrier coefficient, so with respect to this, we can express fusion cross section as the term (2.4), where $S(\epsilon)$ is the astrophysical factor, which is weakly dependent on energy.

$$\sigma(\epsilon) = \frac{S(\epsilon)}{\epsilon} \exp\Big(-\sqrt{\frac{\epsilon_G}{\epsilon}}\Big) \tag{2.4}$$

Cross sections for relevant fusion reactions as functions of energies in centre-of-mass system is shown in Fig. 2.2.

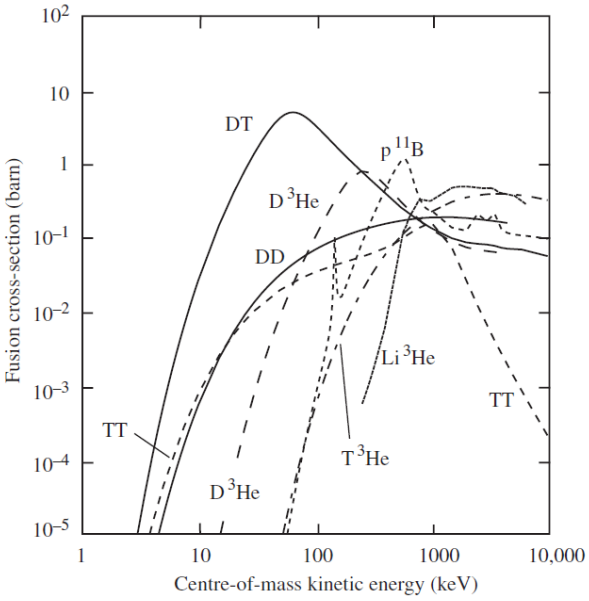

Figure 2.2: Fusion cross sections [2]

2.1.2 Reaction rate

There is another important quantity, which is needed to be mentioned, and it is reaction rate. Reaction rate R is defined by expression (2.5),where σ is the cross section, $|\mathbf{v_1}-\mathbf{v_2}| = v$ is the relative velocity of colliding particles, n_i and f_i is the particle density and the distribution function of particle type $i = 1, 2$.

$$R = \iint \sigma|\mathbf{v_1} - \mathbf{v_2}|f_1 f_2 d^3\mathbf{v_1} d^3\mathbf{v_2} = n_1 n_2 \langle\sigma v\rangle, \quad n_i = \int f_i d^3\mathbf{v_i} \tag{2.5}$$

Reaction rate determines the number of collisions per unit of volume per unit of time, or it answers a question: "How many reactions happen in one cubic meter per second ?". In the expression of reaction rate is quantity $\langle\sigma v\rangle$. This quantity is so called reactivity and for fusion reactions can be expressed as a function of temperature if the distribution functions are Maxwellian (Fig.2.3). From this figure is obvious why fusion community is focused on reaction (2.2a) [2].

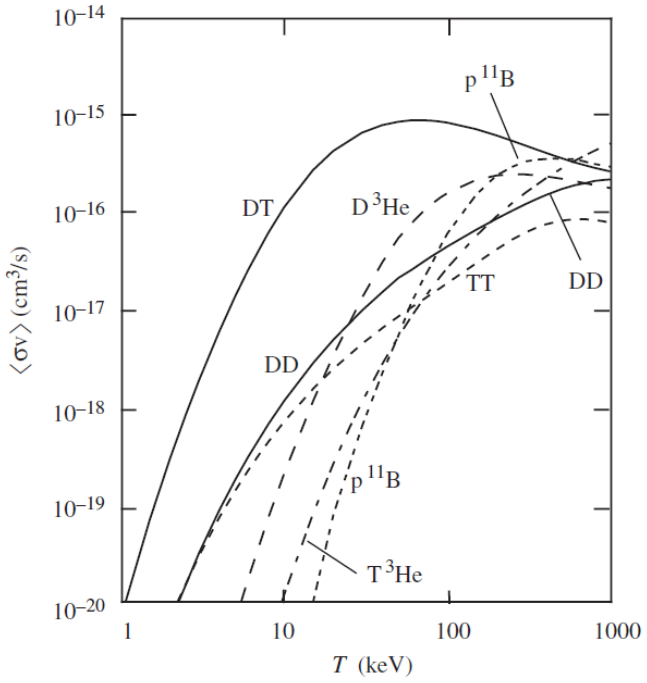

Figure 2.3: Fusion reactivities [2]

2.2 Burning plasmas

There are many technological approaches of how nuclei should fuse together, but one of the most effective approaches is creating the bulk of chaotically moving nuclei with Maxwellian velocity distribution function. The principle of this approach is that chaotically moving nuclei from the tail of distribution function contribute to fusion reactions and released energy from these reactions is being fed back to the Maxwellian bulk of nuclei by Coulomb collisions, covering energy losses by radiation and diffusion. This approach is also called thermonuclear fusion.

As we can see in Fig.2.3, the effective range of temperatures for optimal DT fusion reactivity is around tens of keV. At these temperatures is the arbitrary matter in the state of strongly ionized plasma and at this point is necessary needed to define properties of this state of matter.

2.2.1 Plasma

The term "plasma" was first used by Irving Langmuir in 1927. He used the word plasma because he was reminded of the behavior of blood plasma. The more precise definition of plasma is: "Plasma is a quasi-neutral ionized system of charged particles large enough to behave collectively.". There are also a few more definitions that represent plasma more precisely [1, 3].

- The degree of ionization in plasma is high enough that mean time between collisions with neutrals τ_n is much longer than the period of plasma oscillations τ_{pe}. The basic parameter which is defining these oscillations is so-called plasma frequency ω_{pe} that characterizes the typical time scale of an electron oscillations around the ions.

$$\tau_{pe} = \frac{2\pi}{\omega_{pe}} = 2\pi\sqrt{\frac{\varepsilon_0 m_e}{e^2 n_{e0}}} \ll \tau_n \tag{2.6}$$

- Debye length λ_D of ionized system is much smaller than characteristic plasma dimension l_P. Debye length is a parameter defining a collective behavior of a plasma. At smaller scales than λ_D is plasma defined by the behavior of separate particles.

$$\lambda_D = \sqrt{\frac{\varepsilon_0 kT}{e^2 n_{e0}}} \ll l_P \tag{2.7}$$

- Number of particles in sphere of radius equal to Debye length is high. Dimensionless plasma parameter Λ is large number.

$$\Lambda = 4\pi n {\lambda_D}^3 \gg 1 \tag{2.8}$$

2.2.2 Power inputs

In this section, we are going to discuss processes, which positively contribute to fusion burning plasma by its heating.

First important process in self-sustaining burning plasma is heating by alpha particles created in fusion reactions. With fusion reactions, there are created also neutrons, but they don't contribute to plasma heating because for them is plasma optically thin and they pass through the plasma. These neutrons are latter thermalized by the system of moderators and this energy from neutron slowing down is used in thermal cycle.

Both processes can be represented by terms for alpha particles and neutrons (2.9), multiplying fusion reaction rate (2.5) with the energy of each product of fusion reaction, getting fusion power density. E_α and E_n are energies of alpha particle and neutron released in fusion reaction (2.2a), n_D and n_T are deuterium and tritium particle densities in plasma [2, 4].

$$P_\alpha = n_T n_D \langle \sigma v \rangle E_\alpha, \quad P_n = n_T n_D \langle \sigma v \rangle E_n, \quad E_{fusion} = E_\alpha + E_n, \quad \frac{E_\alpha}{E_{fusion}} = \frac{1}{5} \tag{2.9}$$

Of course, before we achieve the point, where plasma is heating itself by alpha particles, covering energy losses, we need to create conditions of this phenomenon. For self-sustaining burning plasma is needed a temperature of few keV, and for reaching this goal we need to use some additional plasma heating system. Additional heating is pumping energy inside the plasma, increasing its temperature until the plasma is under self-consistent burn. The quantity which defines the process of additional heating is the Q factor, which evaluates how many times is power released by fusion reactions stronger (or weaker) than additional heating.

$$Q = \frac{P_{fusion}}{P_{aux}} \tag{2.10}$$

Q equal to infinity represents the point of ignition, where additional heating is no more needed and the heating process completely relies on alpha particles. There are many types of additional heating (Ohmic heating, injection of neutral particles, radiofrequency heating, laser heating, ...), and this topic we are going to discuss later in a separate section.

2.2.3 Power losses

Of course, as we create high-temperature plasma, we have to take into account processes that are throwing plasma energy away. In this section, we are going to discuss main processes that create power losses in high-temperature plasma.

The first important process is related to the fact that plasma mainly consists of charged particles and charged particles interact with Lorentz force. If a force of any kind affects a body of mass, it causes its acceleration and if charged particle is under acceleration, radiates energy. This is the principle of how plasma loses its energy by radiation.

Charged particles in Maxwellian bulk interact between each other and accelerate themselves.

The radiation is so called "bremsstrahlung" and the power density of this energy loss can be estimated in expression (2.11), where Z is atomic number, n is density of particles and T is temperature of electrons [4].

$$P_{Brem} = C_B Z^2 n^2 [\mathrm{m}^{-3}] \sqrt{T[\mathrm{eV}]}, \quad C_B \cong 1.69 \times 10^{-38} \tag{2.11}$$

Many times we are going to get in touch with plasma confined by external magnetic fields, so it should be appropriate to mention so-called synchrotron radiation. This kind of radiation is caused by cyclotron movement of plasma particles affected by external magnetic fields. Usually, this kind of radiation has a big coefficient of reabsorption in plasma, so this kind of radiation does not take a big part in plasma power losses.

Of course in plasma will also occur impurities (other elements) which will not be totally ionized and may also exist in the excited or deexcited state. Due to collisions with ions and electrons in the plasma, impurity atoms may change their state of excitation and according to this emit photons of deexcitation. This effect also leads to loss of energy by radiation and it is called line radiation. We are able to avoid this effect by maintaining high purity of plasma, especially by avoiding plasma of high atomic number impurities.

Next important kind of power losses are losses by transport. There are many effects, which leads to transport power losses (diffusion, convection, conduction,. . .), but for our purposes, we are going to define them integrally by expression (2.12). The physical meaning of this expression is that the volume-averaged plasma energy density $\bar{w} = \frac{W}{V}$(W is the total plasma energy content and V is the total volume of plasma) is lost by each of mentioned transport processes in characteristic time, so-called confinement time [1, 2].

$$P_{Loss} = \frac{\bar{w}}{\tau_e} \tag{2.12}$$

As we defined processes which are pumping energy inside and blowing outside the plasma, we are standing at the point of defining the criterion of power balance, also well known as Lawson criterion.

2.2.4 Lawson criterion

Criterion defined by John D. Lawson in 1955 was derived from the equation of power balance in a fusion burning plasma system or in a fusion reactor. In our derivation of Lawson criterion, we will not use the same approach as Lawson did, but the consequences which we are about to find out will be very similar.

Let us start with the already mentioned equation of power balance, where power gains and inputs (2.9),(2.10) should be equal or higher than plasma losses (2.11), (2.12), with the perspective of self-consistent plasma burn [2, 5].

$$P_\alpha + P_{aux} \geq P_{Brem} + P_{Loss} \tag{2.13}$$

Assuming D-T plasma composition with concentrations $n_D = n_T = \frac{1}{2}n$, plasma energy density is $\bar{w} = \frac{3}{2}n_i kT + \frac{3}{2}n_e kT = 3nkT$ and that $Z = 1$, we are able to derive from power balance equation equation.

$$\frac{1}{4}n^2\langle\sigma v\rangle\left(\frac{1}{5}+\frac{1}{Q}\right)E_{fusion} \geq C_B n^2\sqrt{T}+\frac{3nkT}{\tau_e} \tag{2.14}$$

After few mathematical manipulations with equation (2.14) we can easily express Lawson criterion (2.15), which express important relation between plasma density n and confinement time τ_e.

$$n\tau_e \geq \frac{3kT}{\frac{1}{4}\langle\sigma v\rangle(\frac{1}{5}+\frac{1}{Q})E_{fusion}-C_B\sqrt{T}} \tag{2.15}$$

Lawson criterion tells us that the plasma density n times confinement time τ_e is quantity, which is needed to be maintained at certain value as a function of temperature. With this purpose is our aim to maintain the product of concentration and confinement time (confinement parameter) in the range of temperatures from 5 to 25keV. To reach this goal is the minimal value of $n\tau_e$ equal to $8.2\times10^{13}\mathrm{cm}^{-3}s$. Confinement parameter as a function of temperature is shown in Fig. 2.4.

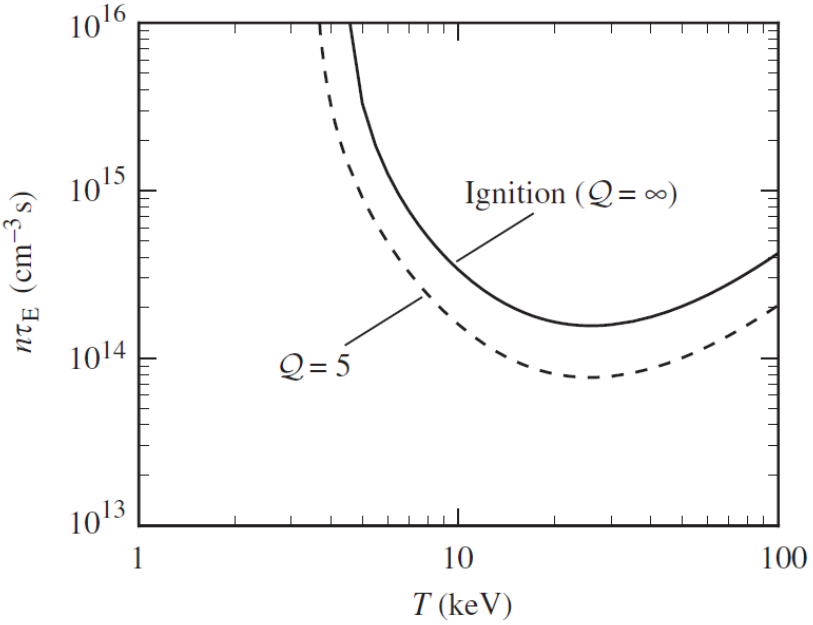

Figure 2.4: Dependency of $n\tau_e$ on temperature T [2]

2.3 Magnetic confinement

According to the Lawson criterion, if our aim is to create energy from fusion reactions by maintaining the Maxwellian bulk of plasma particles, we need to reach product of plasma density and confinement time at the certain value depending on temperature.

It has been mentioned in previous chapters that plasma is state of matter consisting mostly of charged particles and trajectories of these particles can be influenced by electromagnetic fields. This fact can be used for enlarging confinement time, because due to the influence of electromagnetic fields on plasma particles, the effects of transport processes will decrease. In this chapter, we are going to discuss how electromagnetic fields can influence plasma trajectories and confine the plasma in a given volume.

2.3.1 Particle trajectories

The first step of our particle movement description is the nonrelativistic movement of a single particle in a homogenous magnetic field $\mathbf{B}$. For an analytical derivation of this particle trajectory, we will take Newton‘s motion equation for a particle with charge Q and mass m influenced by the Lorentz force (2.16) [6].

$$m\frac{d\mathbf{v}}{dt} = Q\mathbf{v} \times \mathbf{B}, \quad \frac{d\mathbf{r}}{dt} = \mathbf{v} \tag{2.16}$$

If we set z axis of Cartesian orthogonal system in direction of homogeneous magnetic field $\mathbf{B}$, then we can rewrite the solution for velocity and position in expressions (2.17), if the initial conditions are $\mathbf{v_0} = (v_{x0}, v_{y0}, v_{z0})^T$ and $\mathbf{r_0} = (x_0, y_0, z_0)^T$.

$$\begin{pmatrix} v_x \\ v_y \\ v_z \end{pmatrix} = \begin{pmatrix} \cos\omega t & \sin\omega t & 0 \\ -\sin\omega t & \cos\omega t & 0 \\ 0 & 0 & 1 \end{pmatrix} \begin{pmatrix} v_{x0} \\ v_{y0} \\ v_{z0} \end{pmatrix}, \quad \omega = -\frac{Q\mathbf{B}}{m} \tag{2.17a}$$

$$\begin{pmatrix} x \\ y \\ z \end{pmatrix} = \frac{1}{\omega} \begin{pmatrix} \sin\omega t & -\cos\omega t & 0 \\ \cos\omega t & \sin\omega t & 0 \\ 0 & 0 & \omega t \end{pmatrix} \begin{pmatrix} v_{x0} \\ v_{y0} \\ v_{z0} \end{pmatrix} + \begin{pmatrix} x_0 + \frac{v_{y0}}{\omega} \\ y_0 - \frac{v_{x0}}{\omega} \\ z_0 \end{pmatrix} \tag{2.17b}$$

From these expressions (2.17) we can see, that solution for velocity and position has a harmonic character of gyration. These solutions we can split into two parts. The first part of position solution is following magnetic field and the value of particle z coordinate is linearly increasing with time. The second part is gyrating around the z axis with gyration frequency ω and radius R_L, also called Larmor radius (2.18).

$$R_L = \frac{m\sqrt{{v_x}^2 + {v_y}^2}}{QB} \tag{2.18}$$

Let us discuss the consequences of this solution. The trajectory of charged particle in the homogenous magnetic field is a spiral rolled around the magnetic field line and with a radius equal to Larmor radius. If the magnetic field is strong enough, the particle can be confined nearby the magnetic field line. From this point of view, we can imply that diffusion processes are decreased in the perpendicular direction to magnetic field and that was our center of interest. The problem with this concept is that creation of homogenous magnetic field is nonrealistic because it has to be created in infinite space to be homogenous. So we have to involve to our particle trajectory description also weakly spatially inhomogeneous magnetic fields.

To describe the particle movement in a weakly spatially inhomogeneous magnetic field is sufficient to use perturbation theory because the description of particle movement in magnetic fields is difficult in general. Setting Larmor radius as perturbation and neglecting higher than linear perturbations and averaging position over one gyration period in time, we are able to derive the equation for guiding center position R in slowly varying magnetic fields [6].

$$m\frac{d^2\mathbf{R}}{dt^2} = Q\frac{d\mathbf{R}}{dt} \times \mathbf{B} - \frac{Q{R_L}^2\omega}{2}\nabla B, \quad B = |\mathbf{B}| \tag{2.19}$$

This equation is similar to the original motion equation (2.16), except a new diamagnetic term, which is pushing particles (or their guiding centers) out from the region of the stronger magnetic field. Generalizing equation of guiding center with an arbitrary force $\mathbf{F}$ and after vector multiplication of both sides of this equation with vector $\mathbf{B}$, we can derive a drift equation (2.20), where $\left(\frac{d\mathbf{R}}{dt}\right)_\perp$ is velocity component of guiding center vector perpendicular to the magnetic field.

$$\left(\frac{d\mathbf{R}}{dt}\right)_\perp = \frac{\mathbf{F} \times \mathbf{B}}{QB^2} - \frac{m}{QB^2}\frac{d^2\mathbf{R}}{dt^2} \times \mathbf{B} - \frac{{R_L}^2\omega}{2B^2}\nabla B \times \mathbf{B} \tag{2.20}$$

As we can see, assuming slowly varying magnetic field, the particle is no more confined to the magnetic field line, but it also could drift perpendicularly to the magnetic field and it might escape volume of magnetic fields.

There is another important term needed to be defined and it is adiabatic invariant. Derivation of adiabatic invariant (2.21a) consists of evaluating particle kinetic energy change perpendicular to the magnetic field $W_\perp$ (2.21c) during one period of gyration [6].

$$\delta W_\perp = \oint Q\mathbf{E}dl = \iint Q(\nabla \times \mathbf{E}) \cdot \mathbf{dS} = -\iint Q\frac{\partial \mathbf{B}}{\partial t} \cdot \mathbf{dS} \approx \frac{Q{R_L}^2\omega}{2}\delta B = \frac{W_\perp}{B}\delta B \tag{2.21a}$$

$$\frac{\delta B}{B} = \frac{\delta W_\perp}{W_\perp} \implies \frac{W_\perp}{B} = \mu = const. \tag{2.21b}$$

$$\mathbf{v}_\perp = \mathbf{v} - \frac{(\mathbf{v}\cdot\mathbf{B})\mathbf{B}}{B^2}, \quad W_\perp = \frac{1}{2} m {v_\perp}^2 \tag{2.21c}$$

The adiabatic invariant is a ratio of particle kinetic energy perpendicular to the magnetic field and magnitude of magnetic field. As we can see conservation of this quantity and the total kinetic energy of a particle can bring so-called magnetic mirror effect, when a particle of small parallel kinetic energy is bounced back from the region of the higher magnetic field. This effect happens when the condition (2.22) is fulfilled, where ϑ_0 is the angle between velocity and magnetic field B_0, also called pitch angle (Fig. 2.5). The magnetic field is weakly increasing its magnitude along the magnetic field line to the value of B_m (the stronger magnetic field). The ratio of B_0 and B_m is so-called magnetic mirror ratio [6, 7].

$$\sin^2 \vartheta_0 > \frac{B_0}{B_m} \tag{2.22}$$

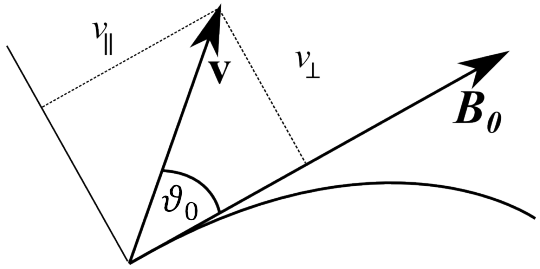

Figure 2.5: Definition of parallel and perpendicular velocity

2.3.2 Magnetohydrodynamics - MHD

Now it is time to discuss approaches to plasma behavior describing if the mean free path of single particles is much smaller than typical plasma dimension and mean collision time is much smaller than the time we are observing plasma.

This problem we are able to avoid if we assume plasma as fluid and instead of describing single particle trajectories and velocities we start to describe the behavior of so-called mass elements. Velocity $\mathbf{u}$ of those mass elements is defined by expression (2.23), which is the center of mass velocity for a mass element, where summation index n is marking particles of species i in the certain mass element. With the term of common behavior of charged particles and its representation through mass elements, we need to define also mass density ρ_m, charge density ρ_Q and current density $\mathbf{j}$ (2.23) [6].

$$\mathbf{u} = \frac{\sum_n m_n \mathbf{v_n}}{\sum_n m_n}, \quad \mathbf{j} = \sum_i Q_i n_i \mathbf{u_i}, \quad \rho_m = \sum_i m_i n_i, \quad \rho_Q = \sum_i Q_i n_i \tag{2.23}$$

Of course, as the title says, we need to involve dynamics into this model. With this purpose, we generalize classical hydrodynamic Euler equations by the density of Lorentz force.

$$\rho_m \frac{d\mathbf{u}}{dt} = \rho_m \left(\frac{\partial \mathbf{u}}{\partial t} + (\mathbf{u} \cdot \nabla)\mathbf{u} \right) = \rho_Q \mathbf{E} + \mathbf{j} \times \mathbf{B} - \nabla p \tag{2.24}$$

The fundamental assumption in MHD is that plasma is quasineutral, which means that $\rho_Q = 0$. Involving this fact back into original equation (2.24), we'll get an equation (2.25).

$$\rho_m \left(\frac{\partial \mathbf{u}}{\partial t} + (\mathbf{u} \cdot \nabla)\mathbf{u} \right) = \mathbf{j} \times \mathbf{B} - \nabla p \tag{2.25}$$

As we can see equation (2.25) has many variables as magnetic field $\mathbf{B}$, kinetic pressure p, velocity $\mathbf{u}$, mass density ρ_m and current density $\mathbf{j}$. For this reason, we need to extend the system of equations with another five equations. The first equation is the continuity equation for mass(2.26).

$$\frac{\partial \rho_m}{\partial t} + \nabla \cdot (\rho_m \mathbf{u}) = 0 \tag{2.26}$$

The second equation is the equation for charge density. The sufficient equation for this concept is Maxwell equation for Ampere's law (2.27) with the approximation of high conductive plasma when the displacement current is neglected.

$$\mathbf{j} = \frac{\nabla \times \mathbf{B}}{\mu_0} \tag{2.27}$$

There are still needed equations for the magnetic field and kinetic pressure of plasma. The equation for the magnetic field we are going to derive from second Maxwell equation for Faraday's law and Ohm's law for fluid matter (2.28).

$$\nabla \times \mathbf{E} = -\frac{\partial \mathbf{B}}{\partial t}, \quad \mathbf{j} = \sigma(\mathbf{E} + \mathbf{u} \times \mathbf{B}) \tag{2.28}$$

Applying rotation on equation (2.27), using equations (2.28) and identities in vector analysis, we are able to get the equation for magnetic field time evolution.

$$\frac{\partial \mathbf{B}}{\partial t} = \frac{1}{\sigma \mu_0} \Delta \mathbf{B} + \nabla \times (\mathbf{u} \times \mathbf{B}) \tag{2.29}$$

Last equation for kinetic pressure cannot be defined generally, so we need a good approximation for its behavior. Sufficient approximation is assumption of polytropic behavior of pressure $p{\rho_m}^{-\kappa} = const.$, where κ is polytropic coefficient. From this equation, we can derive the same kind of equation in differential form.

$$\rho_m \left(\frac{\partial p}{\partial t} + (\mathbf{u} \cdot \nabla)p \right) = p \rho_m \kappa \nabla \cdot \mathbf{u} \tag{2.30}$$

This is the complete system of magnetohydrodynamic equations. Of course for derivation these equations we used a lot of approximations and they don't have to be sufficient in general. For example, description of fast ions generated by neutral beam injection in tokamak plasma can not be described by MHD due to MHD slow time scales. Of course, for many our purposes, these assumptions are safely fulfilled.

2.4 Tokamak

We have already mentioned the physical background of controlled thermonuclear fusion. Now is time to discuss the technical approach, which has been most successful through last decades - Tokamak.

Tokamak is the shortcut of the soviet term: "TOroidalnaja KAmera i MAgnitnyje Katuški", which means a toroidal chamber in magnetic coils. This concept was invited by soviet physicists Igor Tamm and Andrei Sacharov, inspired by the original scheme of Oleg Lavrentiev. In this chapter, we are going to describe basic properties of the most successful technical approach to controlled thermonuclear fusion – Tokamak [1, 5].

2.4.1 Magnetic field configuration

The essential question for controlled thermonuclear fusion is how we are able to confine the high-temperature plasma. It has been mentioned, that feasible way of plasma confinement is the use of the magnetic field because there are no materials which could be exposed to those temperatures. On the contrary, trajectories of plasma particles could be influenced by the magnetic field, so we are about to describe the configuration of magnetic fields in tokamak.

Toroidal magnetic field

The first idea of plasma confinement was a creation of toroidal (axisymmetric) magnetic field, where plasma particles would be gyrating around enclosed circular magnetic field lines. The enclosed magnetic system is also required because of an existence of particles, which parallel velocity is high enough to escape from opened magnetic system (magnetic mirror (2.22)). There is a problem with this concept and in short derivation, we are going to interpret where. Firstly, we should assume the toroidal magnetic field by expression (2.31), where $\mathbf{e_R}$, $\mathbf{e}_\phi$, $\mathbf{e_Z}$ are basis vectors of cylindrical coordinate system.

$$\mathbf{B_T} = 0\mathbf{e_R} + B_\phi \mathbf{e}_\phi + 0\mathbf{e_Z}, \quad B_\phi = B_\phi(R, \phi, Z) \tag{2.31}$$

We can derive that magnitude of the magnetic field decreases inversely with increasing radial coordinate R by involving the Maxwell equations(2.32).

$$\nabla \times \mathbf{B_T} = \mathbf{0}, \quad \nabla \cdot \mathbf{B_T} = 0 \Rightarrow \frac{d(RB_\phi)}{dR} = 0 \Rightarrow B_\phi \sim \frac{1}{R} \tag{2.32}$$

As we can see, the toroidal magnetic field has a non-zero gradient $\nabla|\mathbf{B_T}| = \nabla B_\phi \sim \frac{1}{R^2}\mathbf{e_R}$ and this effect is causing drift motion of plasma particles (2.33), accordingly to equation (2.20).

$$\mathbf{v_D} = -\frac{{R_L}^2 \omega}{2{B_T}^2} \nabla|\mathbf{B_T}| \times \mathbf{B_T} \tag{2.33}$$

This drift motion is polarizing plasma in vertical axis Z by the charge of the particles and this effect is creating a the vertical electric field $\mathbf{E}$ (Fig. 2.6). The creation of this electric field is responsible for another drift motion (2.34), which causes particles escape from the magnetic field.

$$\mathbf{v_d} = \frac{\mathbf{E} \times \mathbf{B_T}}{{B_T}^2} \tag{2.34}$$

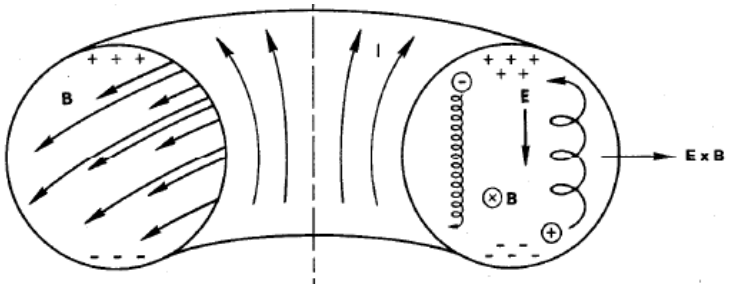

Figure 2.6: Particle drifts in toroidal magnetic field [8]

As we can see, the toroidal magnetic field is not sufficient due to the magnetic field curvature. The magnetic field curvature is responsible for particle drifts, which cause plasma confinement failure.

Poloidal magnetic field

The question is how we can improve mentioned concept. The toroidal magnetic field has an advantage, that it is an enclosed magnetic system and we are still ambitious to keep this concept.

The easiest way of creating enclosed magnetic system is the superposition of toroidal magnetic field and poloidal magnetic field. Poloidal magnetic field lines are also circular but perpendicular to the toroidal magnetic field lines. The superposition of these two components of the magnetic field is the helical magnetic field.

But how is this concept solving the problem of undesirable particle drifts? It has been mentioned that particles can freely move along the magnetic field line and this sight of view recreates a magnetic field line to something like an "equipotential" curve. At the point when the vertical electric field is created by charge polarization of plasma particles in toroidal magnetic field, helical magnetic field enables shorting of the vertical electric field and avoids the mentioned undesirable particle drifts.

So creation of the helical magnetic field appears as right solution of the plasma confinement by magnetic fields, but there is still question of a poloidal magnetic field creation. This problem can be solved by macroscopic electric current in plasma using Ampere's law (2.35), when around a conductor of electric current is poloidal magnetic field.

$$\oint \mathbf{B_P} \cdot \mathbf{dl} = \mu_0 I_P \tag{2.35}$$

Total scheme of the helical magnetic field created in tokamak-like reactors is sketched in Fig.2.7. The same structure of the magnetic field is in a reactor called stellarator, but the

helical magnetic field is created just by an external magnetic coils instead of generating the macroscopic plasma current [9].

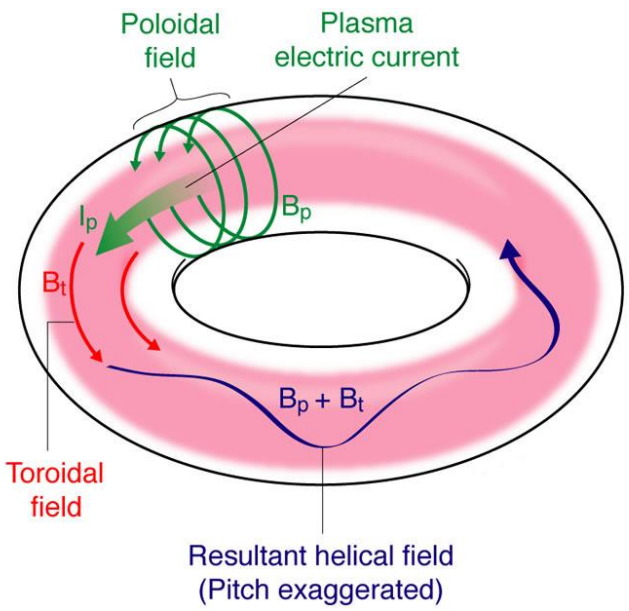

Figure 2.7: Superposition of toroidal and poloidal magnetic field [10]

Vertical magnetic field

The poloidal magnetic field generated by the macroscopic electric current in plasma has also pros and cons. Cons are that the electric current loop is interacting with its own poloidal magnetic field and tends to increase its radius, reaching a minimal potential energy. For this reason, we need to add an external vertical magnetic field, which is compensating the undesirable poloidal magnetic field and it is avoiding the effect of current loop radius growth.

Magnetohydrodynamic equilibrium

Important term in a tokamak description is magnetohydrodynamic equilibrium. It is state of Lorentz force density and gradient of kinetic pressure equivalence (2.36), according to magnetohydrodynamic equation (2.25).

$$\mathbf{j} \times \mathbf{B} = \nabla p \tag{2.36}$$

We are able to imply relations (2.37) from equation (2.36). As we can see, relations (2.37) tell us that current density and magnetic field are perpendicular to gradient of kinetic pressure.

$$\nabla p \cdot \mathbf{B} = 0, \quad \nabla p \cdot \mathbf{j} = 0 \tag{2.37}$$

Considering that gradient of kinetic pressure is perpendicular to surfaces of constant pressure,the magnetic field and the current density are flowing along these surfaces. If we

would be able to determine a shape of those surfaces, we are also able to determine the profile of kinetic pressure and consequently profiles of temperature. So we need to find yet unknown quantity ψ, which is able to fulfill condition (2.38).In an axisymmetric case, this quantity is the toroidal coordinate of vector magnetic potential times radial coordinate. The surface of constant ψ is so-called flux surface [6].

$$\nabla\psi \cdot \mathbf{B} = 0, \quad \psi = -RA_\phi, \quad \mathbf{B} = \nabla \times \mathbf{A} \tag{2.38}$$

Involving this into magnetohydrodynamic equation (2.36), we are able to derive Grad-Shafranov equation (2.39), where I is current which flows in plasma in poloidal direction. Numerical solving of this equation enables us to determine a shape of the flux surfaces. A well-known numerical code used for solving Grad-Shafranov equation in tokamaks is so called EFIT [11, 19].

$$\frac{\partial^2\psi}{\partial Z^2} + R\frac{\partial}{\partial R}\left(\frac{1}{R}\frac{\partial\psi}{\partial R}\right) = \frac{{\mu_0}^2}{8\pi}\frac{\partial I^2}{\partial\psi} + \mu_0 R^2\frac{\partial p}{\partial\psi} \tag{2.39}$$

2.4.2 Construction

Geometry

Tokamak is a toroidal chamber in magnetic coils, so it would be suitable to define basic geometrical parameters that are common for tokamaks worldwide. To describe those parameters we will use a schematic sketch cross section of tokamak axisymmetric geometry in Fig.2.8.

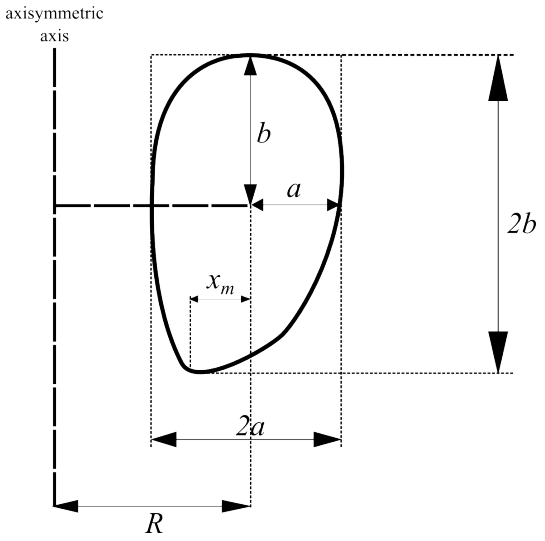

Figure 2.8: Geometrical parameters of tokamak construction

As we can see in Fig. 2.8, the basic parameters of tokamak are the major radius R, the minor radius a and dimensionless quantities such as elongation ε and triangularity κ (2.40). A special set of these parameters determines significant geometrical properties of each tokamak.

$$\kappa = \frac{x_m}{a}, \quad \varepsilon = \frac{b}{a} \tag{2.40}$$

Magnetic coils

In this section, we will discuss basic technical components of a tokamak. The first component is the toroidal coil (or system of toroidal coils) creating the toroidal magnetic field. Generation of the toroidal magnetic field is also just an application of Amperes law.

Secondly, we need to generate an electric current in plasma, to create the poloidal component of the helical magnetic field. With this purpose, we will use a transformer principle, where the second winding of a transformer is the plasma current loop. Of course, achieving of a continual constant plasma current pulse is unfeasible because we need to create the continual increase of magnetic flux in the primary winding. For this reason, there are also needed another plasma current generators (electromagnetic waves, neutral beam injections ...).

The toroidal and poloidal component of the magnetic field cannot acquire arbitrary values. The optimal values for these components we can achieve by fulfilling condition (2.41), where q is so-called safety factor (defined for circular plasma with high aspect ratio R/a). This condition determines MHD stability for the magnetic fields in a tokamak.

$$q = \frac{a}{R}\frac{B_T}{B_P} > 1 \tag{2.41}$$

Third components are poloidal magnetic coils generating the vertical magnetic field, stabilizing the whole plasma current loop, by its positioning and shaping. All the mentioned basic components of a tokamak are shown in (Fig.2.9).

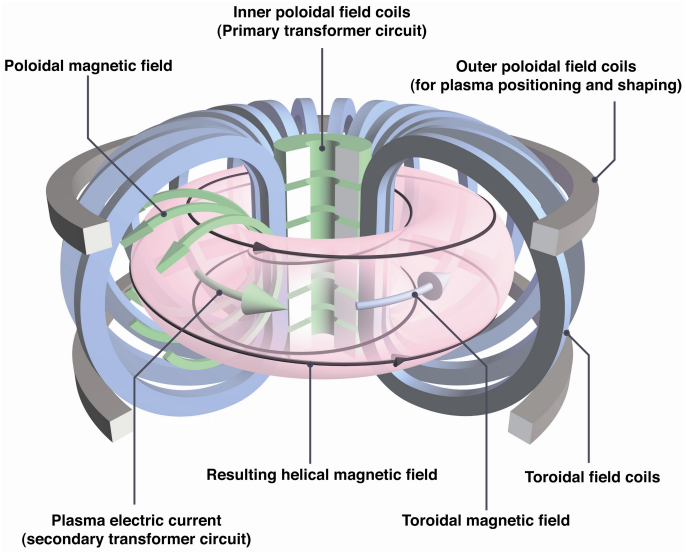

Figure 2.9: Construction components of tokamak [12]

Vacuum vessel

Accordingly to Lawson criterion, we need to create fusion reactor as a system of ultra-high vacuum. For this purpose is necessarily needed vacuum vessel inside the system of magnetic coils, to determine a total reactor plasma volume.

Of course, the temperature of burning plasmas is around hundreds of millions of degrees, so the plasma facing materials of the vessel are expected to endure those temperatures and also should not pollute plasma with impurities. Usual plasma facing materials are tungsten, carbon and beryllium.

2.4.3 Plasma confinement

Confinement time in Lawson criterion is very difficult to determine by a mathematical apparatus in an analytical way. Therefore through the decades of experiments at tokamaks, the confinement time has been investigated as a function of many tokamak parameters empirically. The result of this investigation leads to empirical knowledge of the confinement time by an expression (2.42), where B_T is the toroidal magnetic field at major radius R and M is the average ion mass. Pretty good match between an empirical and an experimental determination of confinement time is shown in Fig. 2.10 for example of scaling (IPB(y,2)) [13], where in the legend are world tokamaks.

$$\tau_e = 0.0562\, I^{0.93} {B_T}^{0.15} n^{0.41} P^{-0.69} R^{1.97} \kappa^{0.78} \varepsilon^{0.58} M^{0.19} \tag{2.42}$$

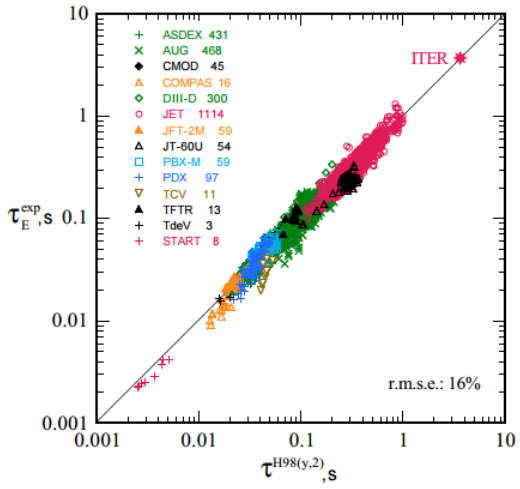

Figure 2.10: Empirical and experimental confinement time comparison

2.4.4 Additional heating

Before the plasma starts to burn self-sustainably, it is needed to insert a certain amount of energy (or power) inside the plasma by an external heating system. The same situation is also in the case of tokamak-like fusion reactors. In this section, we will discuss the most common methods of the additional plasma heating on tokamaks.

Ohmic heating

Historically the first used method of plasma heating was so-called Ohmic heating. This method was based on the Joule's heat release (2.43), when through a conductor of certain resistance flows an electric current and due to collisions between particles is directed flow of particles transferred to their chaotic movement,the internal energy of plasma. The idea of Ohmic heating in tokamaks was to generate electric current in plasma to release enough Joule's heat to heat plasma to thermonuclear temperatures.

$$P = RI^2 \tag{2.43}$$

This heating method is successful, but it is not sufficient for temperatures for fusion plasmas. With increasing temperature of plasma is decreasing plasma resistance, according to Spitzer's resistivity formula (2.44), and released Joule's heat decreases [1].

$$\eta = \frac{\pi Z e^2 m^{\frac{1}{2}} \ln \Lambda}{(4\pi\varepsilon_0)^2 (kT)^{\frac{3}{2}}}, \quad \Lambda = \frac{12\pi}{e^3} \frac{(\varepsilon_0 kT)^3}{\sqrt{n}} \tag{2.44}$$

The Ohmic heating is not sufficient to heat plasma to thermonuclear temperatures. Therefore we also need another additional heating system except Ohmic heating.

Radiofrequency heating

It has been mentioned that a character of particle movement in magnetic fields is harmonic and cyclotron. This fact allows us to deliver an energy to plasma by resonance effects because cyclotron character of particle movement has its characteristic frequency. Generation of an electromagnetic wave spreading through plasma with the frequency required to create the resonance effect at the certain position is so-called radiofrequency heating. Usual wave frequencies used for radiofrequency heating in magnetic confined plasma are ion cyclotron ω_{ci}, electron cyclotron ω_{ce} and lower hybrid frequency ω_{LH} [14].

$$\omega_{ci} = \frac{Ze}{m_i} B, \quad \omega_{ce} = \frac{e}{m_e} B, \quad \omega_{LH} = \sqrt{\omega_{ce}\omega_{ci}} \tag{2.45}$$

Heating by injection of neutral beams

Another well-established approach to heat a plasma is heating by high energetic neutral beams. This approach is based on an acceleration of charged fuel (hydrogen, deuterium, tritium) particles by an electric field outside the reactor vessel. The kinetic energy of these particles is much higher than the energy of particles in plasma and by Coulomb collisions between beam and plasma particles is the total plasma energy increasing due to thermalization of the beam inside the plasma.

The problem of this concept is that we cannot inject charged particles inside a reactor, because as the reactor magnetic fields are confining particles inside the reactor, also those magnetic fields do not allow particles to get inside. For this purpose, we need to neutralize beam particles before they reach the plasma because neutral particles can freely travel through the magnetic fields of a reactor.

After this process, neutral beam particles are ionized by collisions with plasma particles and those high energetic ionized beam particles are thermalized through Coulomb collisions in plasma, increasing the total plasma energy. This approach of additional heating in tokamaks is so called NBI – Neutral Beam Injection and we will pay more attention to this approach in next sections of this thesis [15].

Chapter 3

Neutral Beam Injection - NBI

Neutral beam injection has been already mentioned in the section of tokamak heating systems, but the motivation for the study of this topic is not only heating of tokamak plasma.The importance of NBI is also in the creation of macroscopic electric current by a non-inductive way, tokamak fuel delivery (deuterium and tritium) and study of NBI accompanying physical processes in plasma.

In this chapter, we are going to describe basic physical processes of NBI behavior in plasma and resultant plasma heating, and the basic technological principle of neutral beam creation. We are also going to emphasize important beam and plasma parameters, which have the main influence on resultant beam efficiency. For purposes of this thesis, we are also going to dedicate one section in this chapter to tokamak COMPASS and NBI on tokamak COMPASS.

3.1 Physics of NBI

As the beam of neutral particles is created and injected into a reactor plasma, it is exposed to many physical processes. Firstly, it is exposed to ionization reactions with plasma particles, due to many ionization processes. These ionization processes we are going to describe more precisely in the section of beam ionization. Secondly, there are those fast ionized beam atoms trapped in magnetic fields of a reactor. Trapped fast ions follow their so called drift trajectories and along these trajectories they are exposed to Coulomb collisions with plasma particles or in a worse case, escape from the plasma volume. The processes of fast ion drift trajectories and thermalization of the ionized beam are going to be described in separate sections.

3.1.1 Beam ionization

There are many ionization processes of the neutral beam, but basically, we can distinguish them into three categories.

The first category is ionization processes by electron exchange between a fast neutral beam atom and a plasma ion (3.1a). This process is called charge exchange process (CHX) because electron transfers itself from the fast beam atom to the plasma ion.

Next two categories are ionization processes by an impact of plasma particles (electrons and ions) without any resultant neutral atom. The first process is ionization by ion impact (II) (3.1b) and second is ionization by electron impact (IE) (3.1c). All the mentioned ionization processes can be written into equations (3.1), where the index f and s is marking

fast and slow hydrogen.

$$ {}_{f}H + {}^{+}_{s}H \quad \longrightarrow \quad {}^{+}_{f}H + {}_{s}H \tag{3.1a} $$

$$ {}_{f}H + {}^{+}_{s}H \quad \longrightarrow \quad {}^{+}_{f}H + {}^{+}_{s}H + {}^{-}e \tag{3.1b} $$

$$ {}_{f}H + {}^{-}e \quad \longrightarrow \quad {}^{+}_{f}H + {}^{-}e + {}^{-}e \tag{3.1c} $$

As well as nuclear reactions, ionization reactions have their probability to happen and appropriate quantity of evaluation this probability is the already mentioned cross section. Cross section as a function of deuterium NBI energy for all mentioned ionization reactions is shown in Fig. 3.1 .

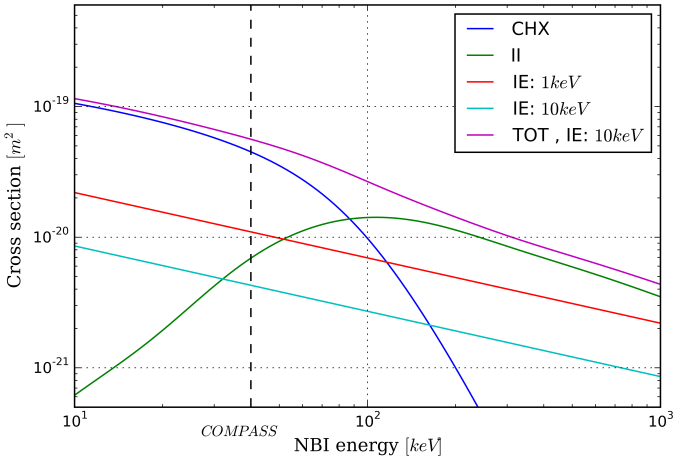

Figure 3.1: Ionization cross sections for deuterium atom [16]

After definition of basic physical quantities, which characterize ionization processes of neutral atoms in plasma, we can derive the differential equation of spatial attenuation of a neutral beam in a plasma (3.2). We can see quantities as electron density n_e (or ion density, because we have taken assumption of $n_e = n_i$), ionization cross sections σ_{CHX} for charge exchange reaction, σ_{II} for ionization by ions and $\frac{\langle \sigma_{IE} v_e \rangle}{v_i}$ for ionization by electrons. In equation (3.2) is also quantity I, so called beam intensity, where N_b is length density of beam particles and v_b is their velocity and x is spatial variable of beam trajectory [1, 15].

$$ \frac{dI}{dx} = -n_e \left(\sigma_{CHX} + \sigma_{II} + \frac{\langle \sigma_{IE} v_e \rangle}{v_i} \right) I, \quad I = N_b v_b \tag{3.2} $$

We can rewrite the analytical solution (3.3a) of equation (3.2) into expression (3.3b), where λ is mean free path of beam atoms, until their ionization.

$$ I(x) = I_0 \exp \left(- \int_0^x n_e \left(\sigma_{CHX} + \sigma_{II} + \frac{\langle \sigma_{IE} v_e \rangle}{v_i} \right) dl \right) \tag{3.3a} $$

$$I = I_0 \exp\left(- \frac{x}{\lambda} \right) \tag{3.3b}$$

The mean free path λ should be comparable with the characteristic dimension of plasma, which is usually proportional to the minor radius of the tokamak. As we can see, the mean free path is also a function of beam atom energy and accordingly to this fact, we cannot set the energy of beam particles arbitrarily. Instead, the energy is chosen based on the plasma parameters, reactor dimensions and geometrical type of injection (tangential injection , perpendicular injection)(Fig. 3.2)

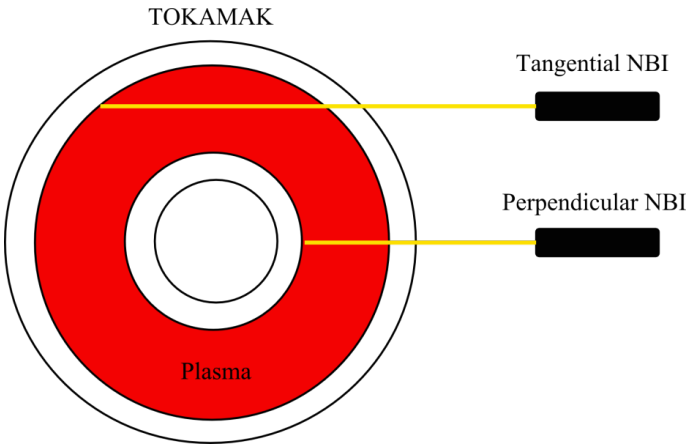

Figure 3.2: Comparison of tangential and perpendicular injection of beam in toroidal cross section

If the energy of the beam atoms is too low, the beam is going to be ionized mostly at the plasma edge and will not heat the plasma efficiently. On the other hand, if the energy of beam atoms is too high, ionization cross sections would decrease rapidly, which would lead to "shine – through" losses of beam [1]. Another kind of losses related to neutralization processes are charge exchange losses, when ionized fast atom is neutralized again and lost from the plasma volume [17].

3.1.2 Drift trajectories

When fast beam atoms become ionized, they are no more neutral and start to interact with external electromagnetic fields of thermonuclear reactor. Trajectories of these fast ions are influenced by many parameters. In this section, we are going to describe the character of these trajectories with respect to those mentioned parameters. After the ionization of a beam atom, we are able to describe its trajectory by using the theory of single particle movement in electromagnetic fields (section (2.3.1)). From the moment of the atom ionization, the fast ion trajectory is predicted by initial conditions of fast ion (initial position and velocity) and the magnetic field configuration of the thermonuclear reactor [15, 18].

The first initial condition is the position where fast atom becomes ionized and it is so called the birth point. If the magnetic fields of the reactor are given, the birth point and the initial

velocity are determining magnetic mirror ratio (2.22) for a certain fast ion. Depending on magnetic mirror ratio we are able to classify ion trajectories into two fundamental categories:

- Trapped ion trajectories
- Passing ion trajectories

Trapped ions are those, whose magnetic mirror ratio is not high enough to enable them to pass through the area of the stronger magnetic field and they are bounced back from this area. In the other words, if the squared ratio of the ion perpendicular velocity to the magnetic field and the total velocity at birth point is higher than the ratio of magnetic field at birth point and the maximal magnetic field reached by the ion, then the ion is "reflected" from the area of stronger magnetic field. Otherwise, if magnetic mirror ratio is high enough, the ion is able to pass through the area of the stronger magnetic field and then we are talking about passing ions.

To describe these fundamental trajectories in tokamak magnetic field configuration, we are going to make computer simulation using Boris – Buneman numerical scheme, due to its sufficient application for simulation of particle trajectories in electromagnetic fields (energy conservation)[6] .For this purpose we used magnetic field configuration of "ideal" circular tomakak, to represent this basic movement behavior. This magnetic field configuration of ideal circular tokamak consists of a superposition of the toroidal magnetic field (2.31) and the poloidal magnetic field generated by the current loop (constant current density used) (2.35). We are going to simulate fast ion trajectories for many different initial parameters. It is good to mention that chosen parameters do not correspond with any realistic case, they were chosen for illustrational purpose. The first simulation will be a comparison of ion trajectories with the birth point at the outer side of tokamak vessel (also called "low field side – LFS", due to decreasing dependency of toroidal magnetic field) and different magnetic mirror ratio (Fig. 3.3).

The first trajectory (left picture of Fig. 3.3) is the trajectory of particle with higher parallel component of velocity (higher magnetic mirror ratio), so we are talking about the passing ion trajectory. Familiar pseudonym for this type of trajectory is also known as "orange" trajectory, due to its circular-like shape of the poloidal projection of ion trajectory.

The second trajectory (right picture of Fig. 3.3) is the trajectory of a higher perpendicular component of velocity (lower magnetic mirror ratio), so this type of trajectory is trapped. Pseudonym of this type of trajectory in the field of tokamak science is "banana" trajectory, due to the banana-like shape of ion trajectory (poloidal projection).

With different magnetic mirror ratios we are getting different types of ion trajectories in tokamak magnetic field configuration. This is crucial for the angle of NBI injection (Fig. 3.2), because perpendicular injection leads to more "banana" trajectories instead of tangential injection. This phenomenon is important for the evaluation of so-called "orbit losses" when particles are lost from tokamak plasma volume while traveling along these trajectories (orbits).

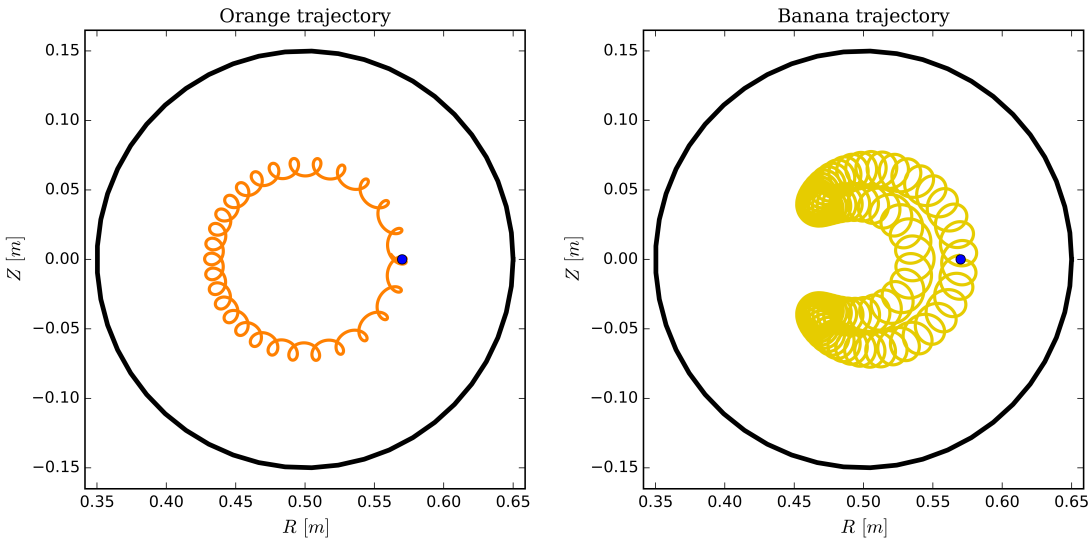

Figure 3.3: Poloidal cross section of particle trajectories with different magnetic mirror ratios

The second simulation will be a comparison of trajectories of particles with the same initial velocities, but different birth points. We are going to observe different movement behavior of particle with the birth point at outer ("Low Field Side - LFS") and inner ("High Field Side - HFS") side of tokamak vessel (Fig. 3.4). If the birth point of a particle is located at HFS, drift trajectory will be still passing, because magnetic mirror ratio will be still sufficiently high.

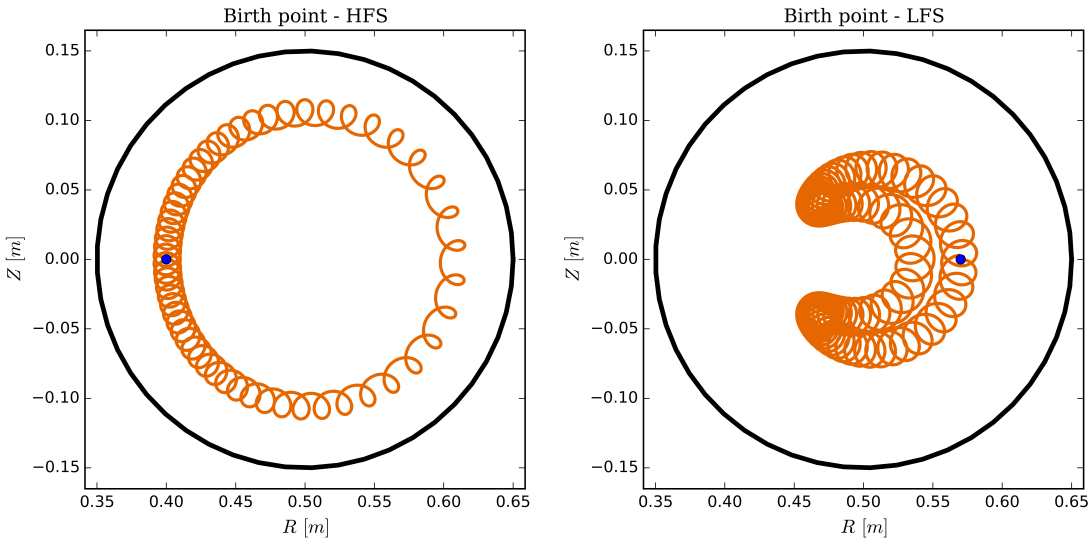

Figure 3.4: Poloidal cross section of particle trajectories with different birth points

After the parameters as birth point and magnetic mirror ratio, we should discuss another parameter, which corresponds to the magnetic field configuration and it is the polarity of the poloidal magnetic field. The different polarity of the poloidal magnetic field implies the

different type of resultant helical magnetic field and also different interaction with charged particles. The polarity of poloidal magnetic field depends on the polarity of the macroscopic electric current generated in tokamak plasma by transformer effect. By this purpose we can distinguish tangential beam injections into another two categories [18]:

- Co - injection
- Counter - injection

Co - injection is the expression for injection of a neutral beam, which is parallel to macroscopic plasma current and counter - injection is the expression for antiparallel injection. The crucial difference between these injections is the polarity of shift Δ of the passing trajectory center from magnetic axis and direction of particle guiding center velocity $\mathbf{v}$. With alternating polarity of plasma, current is alternating the polarity of these quantities. Magnitude of the shift (3.4) is proportional to product of safety factor (2.41) and Larmor radius (2.18) [15].

$$|\Delta| \sim qR_L \tag{3.4}$$

Comparison of poloidal cross sections of beam ion trajectories for co - injection and counter injection is shown in Fig. 3.5.

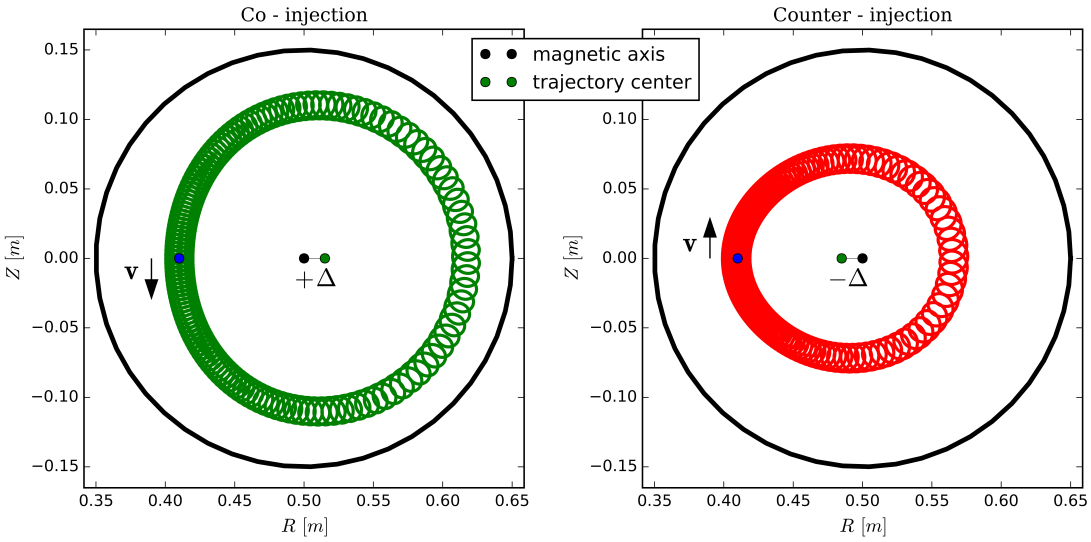

Figure 3.5: Poloidal cross section of particle trajectories for co-injection and counter-injection

The birth point, the magnetic mirror ratio and the orientation of plasma current are most important quantities for beam ion trajectories in a tokamak. For this reason, we are going to make a comparison of these mentioned cases in all 8 combinations ($2^3 = 8$). Comparison of these trajectories is shown in Fig. 3.6. As we can see in Fig. 3.6, if the birth point is located at HFS, the trajectory will be still "orange" shaped in poloidal cross section. "Banana" trajectories occur only in cases of the lower magnetic mirror ratio with the birth point at LFS. The difference in co - injection and counter - injection is recognized in every case.

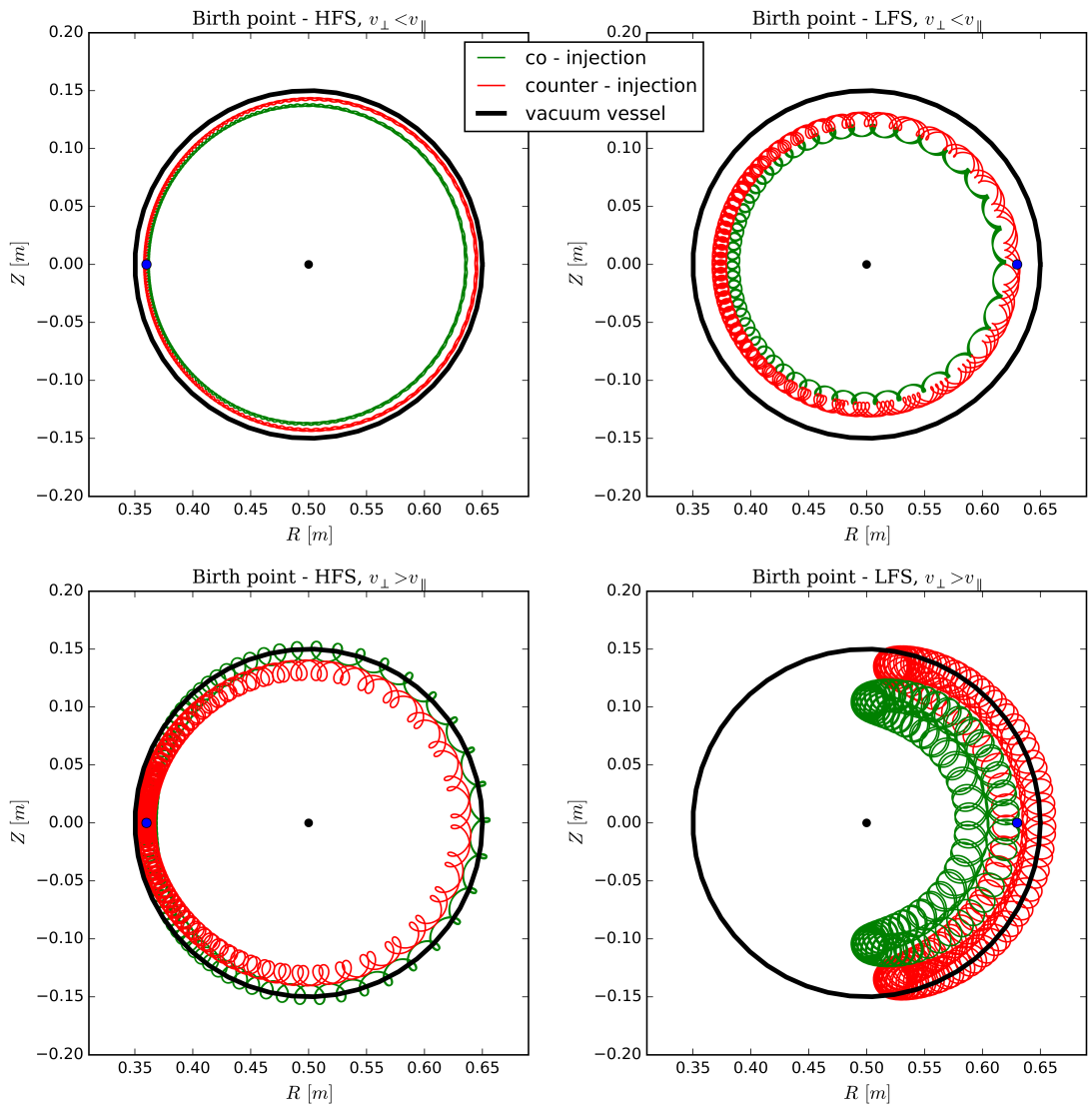

Figure 3.6: Poloidal cross section of particle trajectories for all different cases

In summary, we made a simple simulation to illustrate beam atom trajectory after its ionization. We realized that most important quantities are initial conditions of particle and magnetic field configuration. With the initial condition are most corresponding quantities the birth point (initial position of a particle), the ratio of parallel and perpendicular velocity component to the magnetic field and orientation of the plasma electric current, whose significantly influence the resultant particle trajectory. Knowledge of these quantities is crucial for the determination of so-called "orbit losses" when particle trajectory intersects the surface of a reactor vessel.

3.1.3 Beam thermalization

While fast beam ions are traveling along already mentioned drift trajectories, they are exposed to interactions with plasma particles. The most common interactions are Coulomb collisions with plasma electrons and ions. Due to these Coulomb collisions is the kinetic energy of fast beam ion transferred to electrons and ions, resulting in total plasma heating. In this section, we are going to describe the physical principle of fast beam ion slowing down with resultant plasma heating.

Now we are going to distinguish slowing down processes by collisions with electrons and ions. The first process is the interaction of beam ion with electrons. Due to big difference between ion and electron masses, we can describe slowing down process of beam ion by evaluating friction force F_{be} from the rate of momentum loss by collisions by electrons, where m_b is mass of beam atom, v_b is velocity of beam atom and τ_{se} is slowing down time of beam atom. Thus the power transferred to electrons by collisions with beam ion is given by expression (3.5) [1, 18].

$$P_e = -F_{be}v_b = \frac{m_b {v_b}^2}{\tau_{se}}, \quad F_{be} = -\frac{m_b v_b}{\tau_{se}} \tag{3.5}$$

If we take an assumption that v_b is much lower than electron thermal velocity, we are able to derive τ_{se} from Fokker-Planck equation into expression (3.6), where T_e is electron temperature, m_e is electron mass, e is elementary charge, n is plasma density, $\log\Lambda$ is Coulomb logarithm and ε_0 is permittivity of vacuum.

$$\tau_{se} = \frac{3\sqrt{2\pi}{T_e}^{\frac{3}{2}}}{\sqrt{m_e}m_b A_D}, \quad A_D = \frac{ne^4 \ln\Lambda}{2\pi{\varepsilon_0}^2{m_b}^2} \tag{3.6}$$

After few mathematical manipulations we are able to derive power transferred to electrons by expression (3.7), where $E_b = \frac{1}{2}m_b v_b$.

$$P_e = \frac{2\sqrt{m_e}m_b A_D E_b}{3\sqrt{2\pi}{T_e}^{\frac{3}{2}}} \tag{3.7}$$

The second process, which is needed to be discussed, is the slowing down process by interaction with the plasma ions. This process is different from interactions with electrons because we can not take an assumption that a plasma ion mass is negligible in comparison with a beam ion mass. When the beam ion interacts with the plasma ions, it receives also perpendicular velocity component to the original direction of movement. So we need to correct power transferred to ions of original assumption by adding a new term of perpendicular velocity spreading (3.8) [1, 18].

$$P_i = -F_{bi}v_b - \frac{1}{2}m_b\langle {v_\perp}^2\rangle = \frac{m_b {v_b}^2}{\tau_{si}} - \frac{1}{2}m_b\langle {v_\perp}^2\rangle \tag{3.8}$$

Once again we are able to derive expressions (3.9) from Fokker-Planck equation for ion slowing down time and term of perpendicular velocity spreading with an assumption that beam ion velocity is much higher than the thermal velocity of the plasma ions.

$$\tau_{si} = \frac{m_i}{m_b + m_i}\frac{2{v_b}^3}{A_D}, \quad \frac{1}{2}m_b\langle {v_\perp}^2\rangle = \frac{m_b A_D}{2v_b} \tag{3.9}$$

Using these expressions (3.9) we are able to derive the expression for power transferred from beam ion to plasma ions (3.10), where m_i is ion mass.

$$P_i = \frac{{m_b}^{\frac{5}{2}} A_D}{2^{\frac{3}{2}} m_i \sqrt{E_b}} \tag{3.10}$$

The final expression (3.11) for total direct heating per beam ion we are able to get by summation of expressions (3.7) and (3.10). Total direct heating power per beam ion can be expressed in terms of so-called critical energy E_c by expression (3.12).

$$P = P_e + P_i = \frac{2\sqrt{m_e} m_b A_D E_b}{3\sqrt{2\pi}{T_e}^{\frac{3}{2}}} + \frac{{m_b}^{\frac{5}{2}} A_D}{2^{\frac{3}{2}} m_i \sqrt{E_b}} \tag{3.11}$$

$$P = \frac{2\sqrt{m_e} m_b A_D}{3\sqrt{2\pi}{T_e}^{\frac{3}{2}}} E_b \left(1 + \left(\frac{E_c}{E_b}\right)^{\frac{3}{2}}\right), \quad E_c = \left(\frac{3\sqrt{\pi}}{4}\right)^{\frac{2}{3}} \left(\frac{m_i}{m_e}\right)^{\frac{1}{3}} \frac{m_b}{m_i} T_e \tag{3.12}$$

The term of critical energy is defining the energy of beam ion, which is heating electrons and ions at the same rate. If the energy of beam ion is much higher than the critical energy, electrons are heated preferably. Plasma ions are preferably heated for lower energies of beam ions. This effect is illustrated in Fig. 3.7.

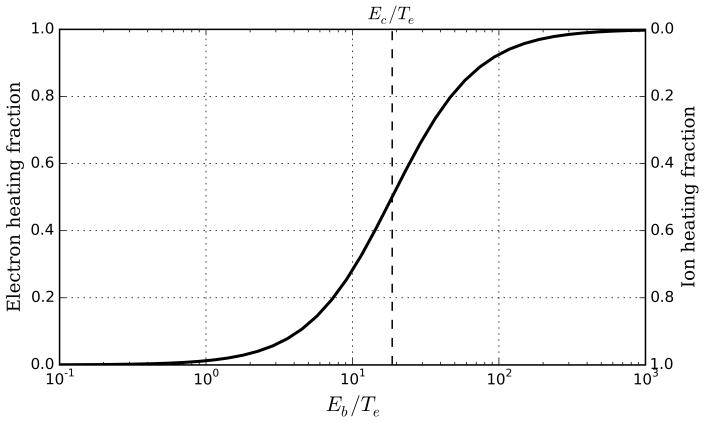

Figure 3.7: Fractions of transferred energy to electrons and ions as function of E_b/T_e

To evaluate the beam ion energy as a function of time, we need to solve the differential equation (3.13). Equation (3.13) defines that negative time derivative of beam energy is equal to total direct power transferred to electrons and ions.

$$-\frac{dE_b}{dt} = P = \frac{2}{\tau_{se}} E_b \left(1 + \left(\frac{E_c}{E_b}\right)^{\frac{3}{2}}\right) \tag{3.13}$$

Solution of this equation we are able to express in term (3.14), where E_{b0} is initial energy of beam ions. This equation is not relevant for very small energies of E_b, but it brings

satisfactory results for time to slow down beam ions to thermal energy. Thus putting $E_b = 0$ we are getting characteristic slowing down time of beam ions by expression (3.15) [1].

$$E_b = E_{b0}\left[\exp\left(-\frac{3t}{\tau_{se}}\right) - \left(\frac{E_c}{E_{b0}}\right)^{\frac{3}{2}}\left(1 - \exp\left(-\frac{3t}{\tau_{se}}\right)\right]^{\frac{2}{3}}\right. \tag{3.14}$$

$$\tau = \frac{\tau_{se}}{3}\ln\left(1 + \left(\frac{E_{b0}}{E_c}\right)^{\frac{3}{2}}\right) \tag{3.15}$$

In summary, we made a short overview of beam ion thermalization process after its ionization. Most important quantity for injected ions is so called critical energy E_c, which determines if beam ion energy is preferably transferred to plasma ions or electrons (Fig. 3.7).

3.2 Technology of NBI

In the previous section, we discussed the basic physical behavior of neutral beam injection inside tokamak plasma. This section is going to be dedicated to the state before the neutral beam reaches tokamak plasma, neutral beam generation, and its basic technological concept. Generation of neutral beam we will describe by subdividing this topic into separate chronological topics:

- Ion source
- Acceleration grids
- Neutralizator
- Bending magnet

3.2.1 Ion Source

Generation of powerful ion beam first requires hydrogen plasma source. This type of source should satisfy several conditions as ion flux density of few tens of amperes per square centimeter, space and temporal uniformity and high content of atomic ions ($\geq$ 80%). These conditions are usually fulfilled by arc discharges or radiofrequency sources [15].

High content of atomic ions is required, because during generation of ions are also generated molecular ions ($^{+}H_2, ^{+}H_3, ^{+}D_2, ^{+}D_3 \ldots$). These molecular ions are after acceleration at the same energy as atomic ions, but after their dissociation, their kinetic energy is redistributed to dissociation fragments. This effect is responsible for the existence of nonmonoenergetic particles of energy E_0, but also particles of energy $E_0/2$ and $E_0/3$ and higher fractions in beam composition. The content of higher fractions of the beam composition usually decreases with the increasing power of injection [18].

3.2.2 Acceleration grids

It was mentioned before, that ions from the ion source are accelerated by a system of electrostatic acceleration grids. At this region, ions acquire the same energy E_0. Acceleration grids conventionally consist of three or four insulated metallic electrodes with appropriate voltages for acceleration. One of the electrodes is negatively charged to repel electrons generated in neutralizer. Electrodes are usually curved for appropriate beam focusing inside the tokamak plasma.

3.2.3 Neutralizer

After ion acceleration, is his trajectory directed to neutralizer. Neutralizer is part of NBI device where ions become neutral due to charge exchange process mentioned in section (3.1.1). Neutralizer is a chamber filled with working gas (usually hydrogen isotopes), which molecules are used for neutralization reactions (3.1) with accelerated ions.

The problem which occurs at this point is that generated neutral atoms in neutralizer might become ionized again due to next collisions with working gas of neutralizer. This effect leads to the fact, that total efficiency of beam neutralization is not hundred percent, but it is dependent on the concentration of working gas, thickness of neutralizer cell and neutralization and ionization cross sections.

Due to ionization cross sections, the efficiency of neutralization is decreasing with increasing energy of accelerated ions. This reason leads to the application of negatively charged ions for NBI at larger devices (ITER, DEMO, ...) because neutralization cross sections for negative ions at those energies are much higher than for positive ones [20].

3.2.4 Bending magnet

It was mentioned that neutralization efficiency is not hundred percent, and this fact brings the effect of the beam of non-neutralized ions leading their way out of the neutralizer. The flow of these ions is needed to be bent off the trajectory of neutrals, and this is fulfilled by applying bending magnet in the way of ions. Bending magnet has an influence on ion trajectories and ions are bent away to the ion dump. Due to the high power of bent ion flow is needed cooling of ion dump.

Scheme of NBI components is shown in Fig. 3.8.

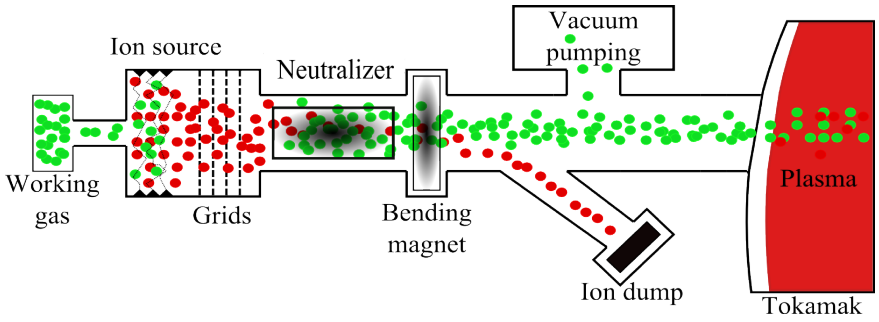

Figure 3.8: Scheme of NBI components

3.3 Tokamak COMPASS and NBI

This thesis is focused on effects of NBI on tokamak COMPASS, therefore we need to describe basic properties and parameters of this tokamak and its NBI systems.

Tokamak COMPASS is the biggest tokamak of Czech Republic and is situated at Institute of Plasma physics AS CR. The importance of tokamak COMPASS we are going to assign to its geometrical similarity with bigger tokamaks (JET, ITER, ...). Besides similarity with bigger tokamaks, one of the big precedences of tokamak COMPASS is the flexibility of generation various magnetic field configuration. Basic technical parameters of tokamak COMPASS are noted in Tab. 3.1 [21].

Major radius	0.56m
Minor radius	0.20m
Plasma current	400kA
Toroidal magnetic field	$0.8 - 2.1$T
Plasma duration	~ 1s

Table 3.1: Basic parameters of tokamak COMPASS

NBI is heating method used on tokamak COMPASS and it is the main topic of this thesis. Tokamak COMPASS is equipped with two tangential neutral beam injectors, each of power 300kW and ion energy $E_0 = 40$keV. Overview of parameters of NBI systems used on tokamak COMPASS are shown in Tab. 3.2 [22].

Ion energy	40keV
Ion current	2×12.5A
Total power of injected neutrals	300kW
Pulse duration	300ms
Beam diameter	7cm
Total input power	1.5MW

Table 3.2: Basic parameters of COMPASS NBI systems

Chapter 4

NBI simulations

Numerical simulations play a great role in the understanding of tokamak experiments. Simulations are able to verify consistency of experimental data from diagnostic systems, or even additionally calculate quantities, which are not directly measured. If a numerical model is one of the "well trained" at experimental data, we are able to use this model to predict parameters of future experiments. This chapter is going to be dedicated to numerical simulation models and their comparisons focused on simulations of NBI in tokamaks. We decided to use input data from plasma discharge (shot number: 10338) of tokamak COMPASS for comparison of our simulations.

4.1 Simplified ionization model

One of the points of this thesis was the development of a simple ionization model of NBI applied for plasma discharges on tokamak COMPASS. This model was based on solving equation (3.2) for parameters of tokamak COMPASS. To solve the equation (3.2), we need to define input data such as the geometry of the neutral beam in the tokamak, profiles of electron density along the beam trajectory and ionization cross sections as a function of NBI and plasma parameters.

The geometry of a single beam of an infinitesimal width is described by Fig. (4.1). The geometry is described by parameters R_0, ϕ_0, z_0 of starting point of the beam in coordinates of a toroidal coordinate system, the tangency radius of the beam a and the inclination angle θ from the mid plane ($z = 0$). The variable x describes length of the beam trajectory.

The second quantity we need to define is the electron density profile along beam trajectory. We know that at flux surfaces (surfaces of constant poloidal magnetic flux) are quantities as temperature and density constant and this fact enable us to define a profile of electron density along NBI trajectory axis. We can define the trajectory of NBI in toroidal coordinates as a function of the beam trajectory variable x. The poloidal magnetic flux ψ is calculated as a function of these toroidal coordinates from Grad-Shafranov equation (2.39), thus we are able to define ψ as a function of x. The last question is how we are able to define the electron density as a function of ψ.

For our purpose, we can parametrize electron density by (4.1), where n_{IN} is the central electron density, n_{OUT} is the electron density at plasma edge, α and β are dimensionless

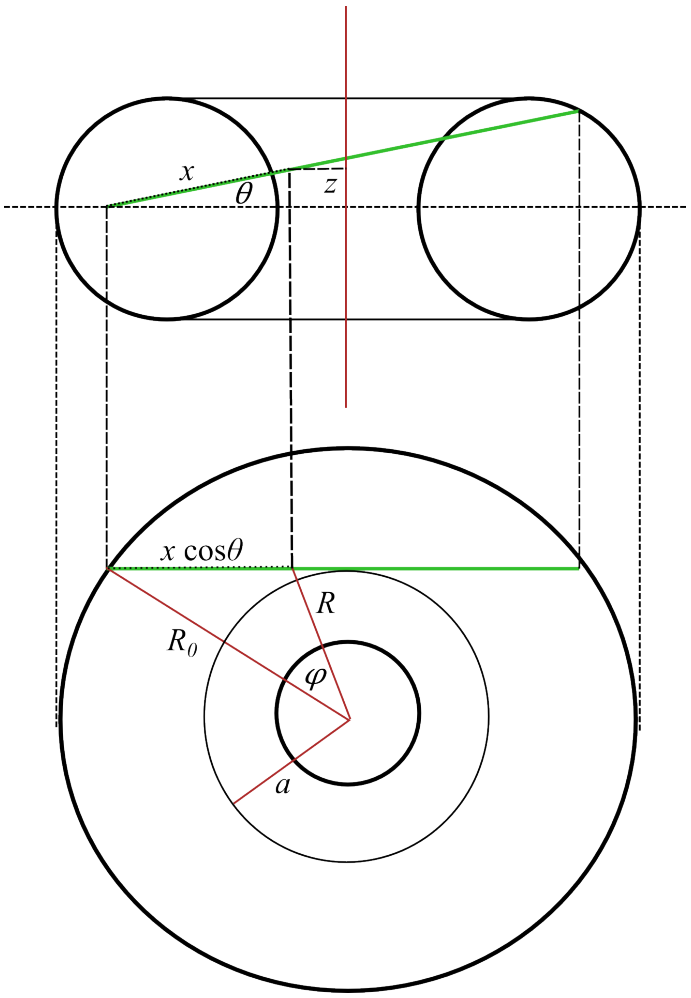

Figure 4.1: Scheme of NBI geometry in simplified ionization model

parameters and ρ is normalized ψ defined by expression in equation (), where ψ_{IN} is value of poloidal magnetic flux at plasma center and ψ_{OUT} is value of poloidal magnetic flux at plasma edge. n_{IN}, n_{OUT} and dimensionless parameters α and β are calculated by the least square fitting method from Thomson scattering diagnostic of electron density.

$$n_e = (n_{IN} - n_{OUT})\left(1 - \rho^{\beta}\right)^{\alpha} + n_{OUT}, \quad \rho = \sqrt{\frac{\psi - \psi_{IN}}{\psi_{OUT} - \psi_{IN}}} \tag{4.1}$$

Last but not least quantity, which is needed to be defined is ionization cross section for particular ionization processes. We took the fitted functions of ionization cross sections as functions of beam atom kinetic energy from Kikuchi, Lackner, Tran. Fusion Physics (Fig. 3.1)

After the definition of geometry,the electron density and the ionization cross sections we were able to create first simulation of single beam attenuation. Single beam has an infinitesimal width and the geometry of tangential injection: $z_0 = 0m$, $\phi_0 = 0$, $R_0 = 0.78m$, $a = 0.56m$ and $\theta = 0$. Profile of electron density and profile of beam intensity attenuation

along the beam axis are shown in Fig. 4.2. We can see in Fig. 4.2 typical exponential dependency of the beam along the beam axis according to equation (3.3b).

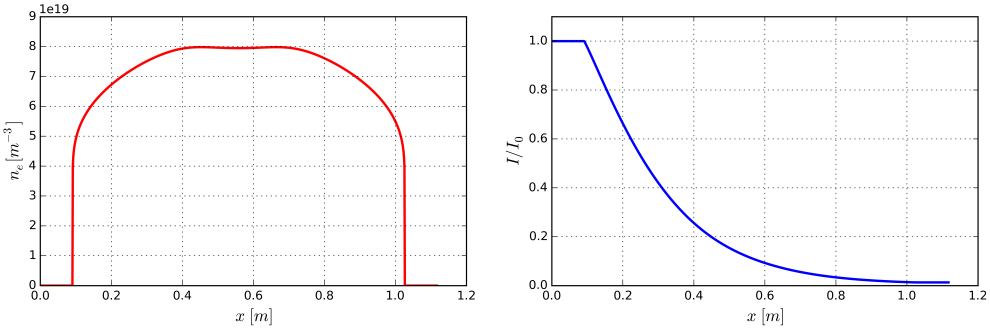

Figure 4.2: Profile of electron density and beam attenuation along the beam axis

Beam intensity attenuation has been calculated numerically by Python Scipy library functions (Runge-Kutta ordinary differential equation solver). The first parametric study we are able to create with this model is the evaluation of shine through losses with increasing of central density and increasing beam atom energy. The result of this parametric study is shown in Fig. 4.3 . Shine through losses are almost negligible (max 10%) in the case of typical tokamak COMPASS environment ($n_{IN} > 5 \times 10^{19}\mathrm{m}^{-3}, E_0 = 40\mathrm{keV}$).

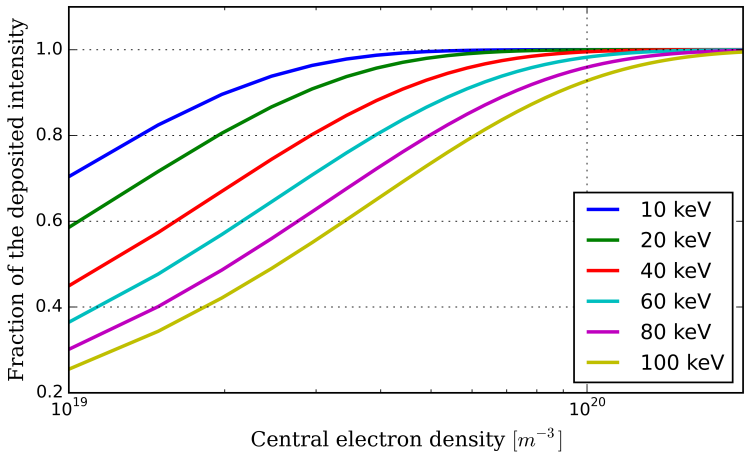

Figure 4.3: Parametric study of deposited beam intensity in plasma as function of n_{IN}

We can calculate the spatial distribution of ionized beam power, i.e. the fraction of total beam power deposited in volume between neighboring flux surfaces. This quantity has a dimension of power density and is denoted H. The evaluation of the quantity H for separate beam atom energy fractions of total beam power ($0.3MW$) is shown in Fig. 4.4. We can see that the major contribution to total H profile has E_0 energetic beam component, so $E_0/2$ and $E_0/3$ components do not play a great role at these beam powers (section 3.2).

The single beam model of infinitesimal width is just the first approximation to real physics hidden behind NBI ionization. For this reason, we need to create a better approximation

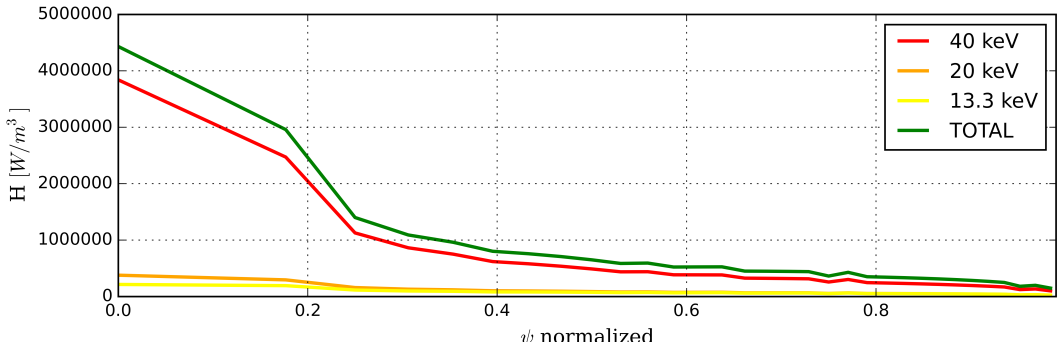

Figure 4.4: Radial profiles of H for particular energetic beam components ($E_0 : 0.77, E_0/2 : 0.13, E_0/3 : 0.10$)

of real NBI ionization by involving the finite beam width. We are able to simulate this effect by superposition of several infinitesimal beams of the same intensity and power with the total intensity of the original beam. The geometry of this generalized model consists of the superposition of 9 beams distributed in the beam front. Beam front is subdivided into 9 regions of the same area and particular beams are situated into surface centers of this regions (Fig. 4.5)

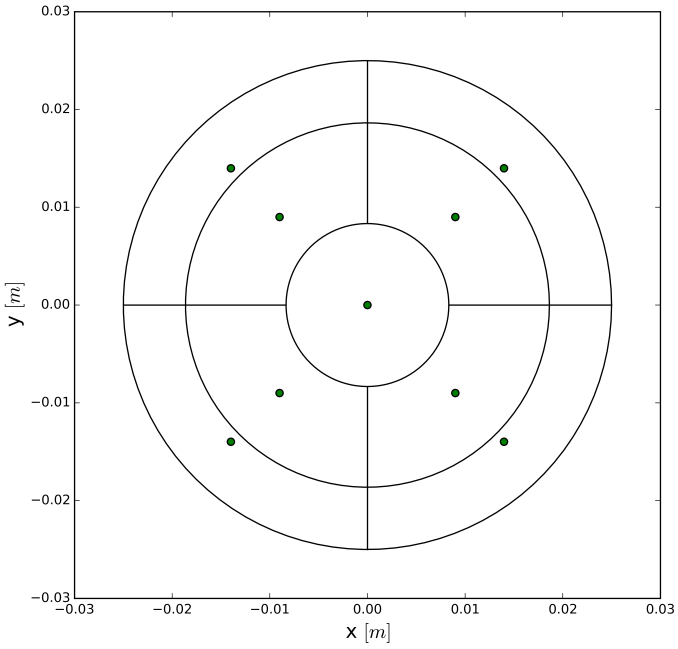

Figure 4.5: Geometry of the beam front

Visualization of the beam relative to the tokamak COMPASS geometry in poloidal and toroidal cross-section is shown in Fig. 4.6 . We can see poloidal cross section positions of

the beam along the beam axis and also cross sections of flux surfaces.

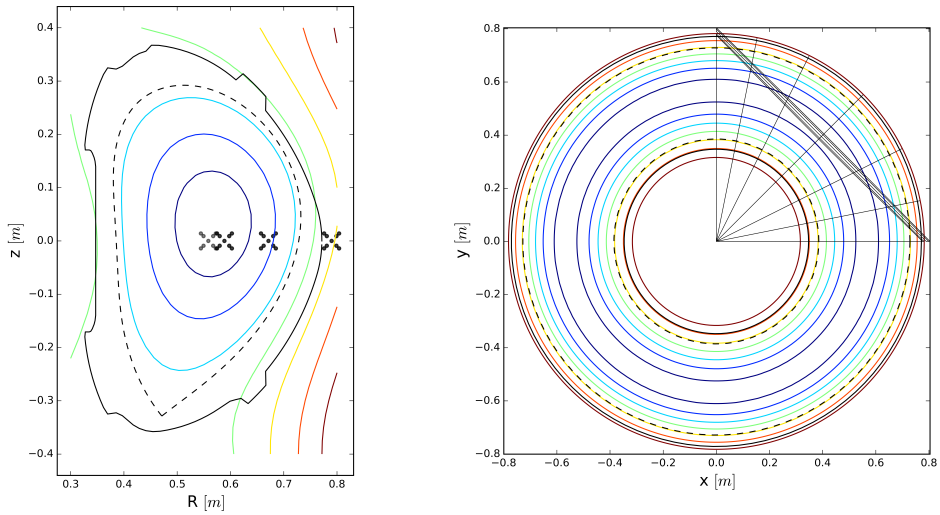

Figure 4.6: Visualisation of the beam in poloidal a toroidal cross section

Generalization of the beam spatial distribution in beam front has made a difference in the profile of quantity H. As we can see, the tail of the H radial dependency is in both cases almost the same but the maximum is slightly shifted from the plasma center.

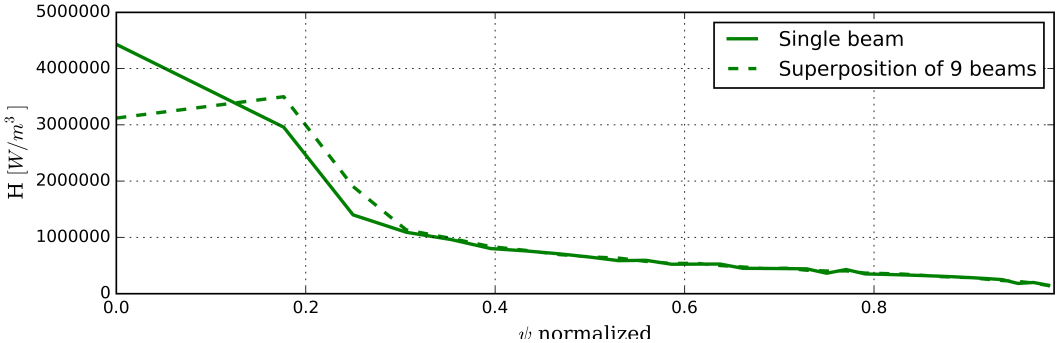

Figure 4.7: H profiles for single beam and superposition of 9 beams

The difference between models lead us to question what is the effect of the width of 9 beam model and the calculated deposited ionized power in the plasma. For this purpose, we have made a parametric study of the deposited power fraction from the beam as a function of the beam radius for different energies E_0. The result of this study is shown in Fig. 4.8. As we can see, the beam radius of 9 beam superposition model does not play a big role in case of typical tokamak COMPASS environment (Beam radius = $5cm$).

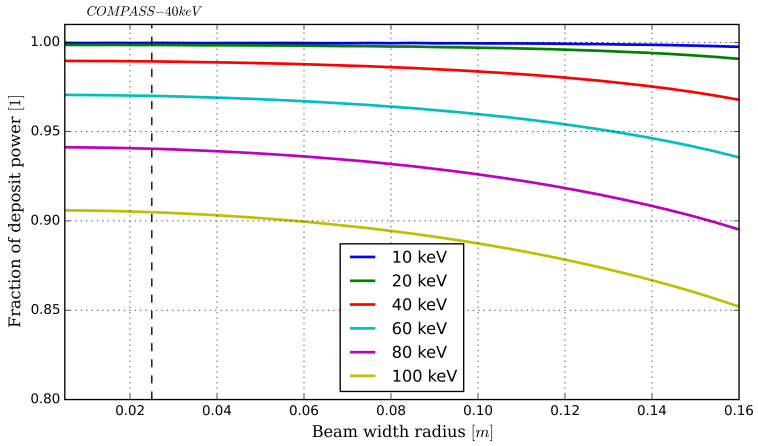

Figure 4.8: Deposited beam intensity in plasma as function of the beam width radius

In summary, we made a simplified model of neutral beam ionization in tokamak COMPASS plasma environment. After the definition of beam geometry, electron density along the beam axis and ionization cross sections for beam atom energies, we were able to create the first parametric studies with this simplified model. The result of these parametric studies has shown us that shine through losses are for typical tokamak COMPASS plasma parameters almost negligible (max 10%) (Fig. 4.3). Another fact we acquired was that contribution of higher energetic beam components ($E_0/2$ and $E_0/3$) do not play a significant role in profiles of ionized power density H (Fig. 4.4). We have made correction of this simplified model by involving the superposition of 9 infinitesimal beams of the same intensity instead of one beam of total intensity. This correction has been recognized at H profile (Fig. 4.7).

4.2 Integrated Tokamak Modelling

For purposes of experimental support by this thesis, we decided to use sophisticated simulation models of NBI. We decided to use modelling apparatus from the EUROfusion integrated modelling effort (EU-IM) which is a successor of EFDA (European Fusion Development Agreement) taskforce [23].

BBNBI (Beamlet Based NBI) code was used for Monte Carlo computation of beam ionization and RISK (Rapid Ion Solver for toKamaks) code for simulating the evolution of the distribution function of NBI plasmas. BBNBI calculation of the beam ionization is creating an ensemble of fast test ions assigned to RISK distribution function calculation.

We needed to create input data structure to utilize with these simulation codes. Data structure for these codes is so called CPO (Consistent Physical Object), which means data structure that contains the relevant information on a physical entity. The CPO-s for our purposes had to contain information about neutral beam injector parameters (geometry, total power,E_0 energy, beam composition power and current fractions, ...), tokamak vessel geometry, profiles of plasma quantities (densities, temperatures, magnetic field, ...) and

magnetohydrodynamic equilibrium calculated by Grad-Shafranov equation [19].

4.2.1 BBNBI

BNBI follows neutrals from the injector until they are ionized, producing an ensemble of fast test ions and unlike codes that have earlier been used for beam ionization, BBNBI can calculate ionization even outside the last closed flux surface.

Neutral beam injectors in tokamaks are based on a similar technological structure mentioned in section (**??**): an ion source connected to an electrostatic accelerator is followed by a neutralizer and a residual ion dump. BBNBI follows the neutral particles starting from the last accelerator grid.

The beam is modeled as a set of separate sub-beams, or beamlets, one from each grid hole in the grounded grid. The fine structure of the beam is taken into account by defining the location and direction of each beamlet individually. The BBNBI beamlet geometry for COMPASS tokamak has been used the same as in the case of the simplified model of 9 beam superposition. (Fig. 4.6). The other adjustable parameters are:

- Injected particle species (H, D, T)
- Total NBI power
- First energy component E_0
- Fractions of particles in the different energy components $E_0, E_0/2$, and $E_0/3$
- Beamlet divergence

After the definition of initial parameters, neutral atoms are generated with starting location at the last accelerator grid. The neutral atom is assigned a velocity in the direction of the beamlet, offset according to the beamlet divergence, and moved along its velocity vector until it either hits an obstacle (beam scrapers and the edges of an aperture) or enters the vacuum chamber.

Inside the device, the neutral particle is assigned a uniformly distributed random ionization threshold $\lambda \in [0, 1]$ and it is pushed along a straight trajectory while simultaneously evaluating the cumulative ionization probability P (4.2),

$$P(s) = 1 - \exp\left(- \int_0^s \Sigma(\xi) d\xi \right) \tag{4.2}$$

where s is the distance along the neutral atom trajectory and Σ is the total effective ionization cross-section. In the code, the integral is discretized into small steps such that Σ can be taken constant between neighboring points s_i and s_{i+1}. The probability P_i of ionization before s_i is then determined by expression:

$$1 - P_i = (1 - P_{i-1}) \exp\left(\Sigma_i (s_i - s_{i-1})\right) \tag{4.3}$$

where $P_0 = 0$ and $\Sigma_i = (\Sigma(s_i) + \Sigma(s_{i-1}))/2$. Once $(1 - P_i)$ decreases below the random threshold λ, the last step is retaken and the exact ionization point s_f is computed from expression:

$$s_f - s_{f-1} = -\frac{1}{\Sigma_f} \ln\left(\frac{\lambda}{1 - P_{f-1}}\right) \tag{4.4}$$

After this step a test particle is recorded. If the wall is encountered before $1 - P_i < \lambda$, the neutral particle is considered shine-through [24].

4.2.2 RISK

The RISK code solves the bounce-averaged Fokker–Planck equation derived from the gyro-averaged Fokker–Planck equation (4.5), where f is the distribution function as function of W (the kinetic energy), μ (the adiabatic invariant), ρ (the flux surface label) and θ (an angle determining the poloidal position along a flux surface).

$$\frac{\partial f}{\partial t} + \mathbf{v_g} \cdot \nabla f = C(f) + S - L(f) \tag{4.5}$$

In equation (4.5) is $\mathbf{v_g}$ the guiding center velocity, In equation (4.5) is $\mathbf{v_g}$ the guiding center velocity, $C(f)$ is the collision operator, S is a source term representing the ionization source of injected neutral beam ions and $L(f)$ is a particle loss term.

Two simplifying assumptions are made with solving of equation (4.5). The first assumption is that we assume the analysed ions to be in the banana regime (does not mean that the analysed ions are trapped in banana trajectories, but in state of a low collisionality regime) and the second one is that the banana width is negligible, in other words, we adopt the zero banana width approximation. Consequently, the bounce time between magnetic mirrors τ_b is much shorter than the collisional time scale τ_c, thus can be utilized this separation of time scales by expanding the distribution function in a τ_b/τ_c series, where f_0 is the distribution function of the unperturbed orbit and f_1 represents a small perturbation.

$$f = f_0 + \frac{\tau_b}{\tau_c} f_1 + \dots \tag{4.6}$$

Now it is time to define the bounce average operator as the integral along the orbit:

$$\langle \cdots \rangle = \frac{1}{\tau_b} \oint (\cdots) \frac{d\theta}{\mathbf{v_g} \cdot \nabla \theta} \tag{4.7}$$

Inserting expansion (4.6) into the equation (4.8) and applying the bounce-averaged operation (recognizing that f_1 must be periodic in θ) leads to 0th-order bounce averaged Fokker–Planck equation solved by RISK.

$$\frac{\partial f_0}{\partial t} = \langle C(f_0) \rangle + \langle S \rangle - \langle L(f_0) \rangle \tag{4.8}$$

However, completely neglecting finite orbit width effects can lead to inaccuracies when calculating the profile dependence of particular quantities. The method used in RISK is distributing the source according to the fraction of time that ion stays at different flux surfaces during its orbit after ionization. An important feature of the procedure is that it enables for a fairly accurate evaluation of first ion orbit losses. If the orbit following detects that an ionized particle intersects a material surface during its first orbit, the contribution from the associated source is taken to be lost [25].

4.3 METIS

The METIS (Minute Embedded Tokamak Integrated Simulator) code has been developed to simulate tokamak plasma temporal evolution using information from scaling laws chained with simplified source models and using an almost always convergent computing scheme that enables to simulate a full plasma discharge in a time of approximately one minute.

METIS includes many particular solvers based on scaling laws, simplified analytical formulations. Separate solver blocks and their cooperation are shown in Fig.(4.9).

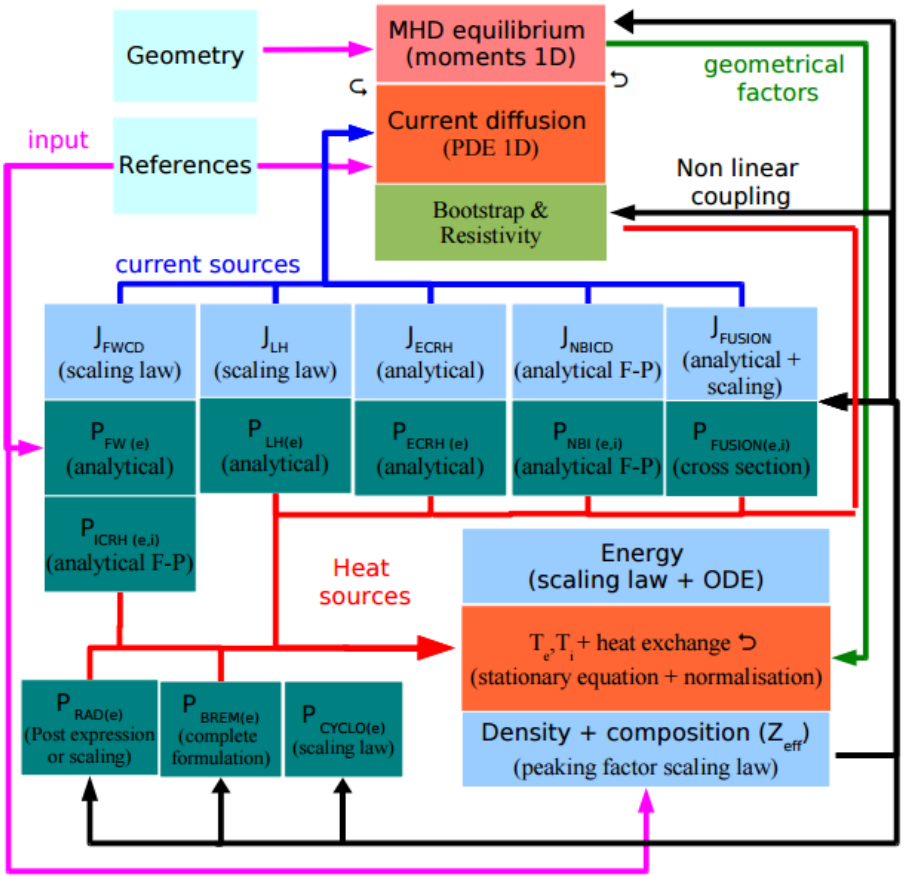

Figure 4.9: Separate solver blocks and their cooperation in METIS

We are not able for purposes of this thesis to describe the principle of the separate particular block, therefore we are going to focus on blocks which are directly related to neutral beam injection.

The first quantity which should be mention with NBI heating is plasma energy. The energy content of the plasma is given by a scaling law that depends on the scenario. At this point, we should define METIS power balance equations. First equation is definition of total input power (4.9), where P_α is the alpha particles power contribution, P_ω is ohmic power, P_{ICRH} is the ion cyclotron resonance heating power, P_{LH} is the lower hybrid radiofrequency power, P_{NBI} is the neutral beam injection power and P_{ECRH} is the electron cyclotron resonance

heating power.

$$P_{in} = P_{\alpha} + P_{\omega} + P_{ICRH} + P_{LH} + P_{NBI} + P_{ECRH} \tag{4.9}$$

Second equation is definition of loss power (4.10), where $Pbrem$ is the bremsstrahlung radiative power, P_{cyclo} is the power lost by cyclotron radiation and P_{line} is the total radiative power due to line radiation, λ_{line} is the fraction of line radiation power coming from the core plasma. $\frac{dW}{dt}$ is the expression, which corresponds with magnetic energy.

$$P_{loss} = P_{in} - P_{brem} - P_{cyclo} - \lambda_{line} P_{line} - \frac{dW}{dt} \tag{4.10}$$

Total energy content W_{th} is calculated by ordinary differential equation (4.11), where τ_E is already mentioned energy confinement time. Confinement time is given by scaling law, which can be chosen by type of confinement regime. Commonly used scaling law (2.42) has been mentioned in section (), but we are able to set scaling law according to our purposes. Confinement time could be modified by the dimensionless time-dependent quantity called H factor, which is linearly increasing value confinement time.

$$\frac{dW_{th}}{dt} = -\frac{W_{th}}{\tau_E} + P_{loss} \tag{4.11}$$

Solving of the time dependent equation for total energy content is the first part of evaluation heat transport. The second part consists of solving the time-independent transport equations (4.12), where T_e and T_i are the electron and ion temperatures κ_e and κ_i are electron and ion thermal conductivities and J_e and J_i are electron and heat fluxes.

$$J_e = -\kappa_e \nabla T_e, \quad J_i = -\kappa_i \nabla T_i \tag{4.12}$$

At this point, we should describe heating and current drive by NBI calculated by METIS. The beam attenuation is computed for a few sub-beams by solving an equation (3.2). In METIS, the neutral beam path is taken in the equatorial plane of the plasma (at $Z = Z_0$) and the radius of tangency is prescribed ($R_{tan} = a$). The final value of the beam intensity determines shine through losses.

From ionization power deposition is subtracted first orbit losses computed from a simplified model. Firstly is supposed that the most of the fast ions are trapped nearby the plasma edge and then is computed drift orbit width δ_0. If initial position of created fast ions is smaller than δ_0, fast ions are lost. From ionization power deposition is calculated power transferred to ions according to equation (3.10) [26].

4.4 Comparison of simulations

This section is going to be dedicated to the comparison of particular models mentioned before. The purpose of creating this section was to realize advantages and disadvantages of particular models for better experimental support. We are going to compare ionization power profiles of simplified ionization model and BBNBI code and power transferred to electrons and ions calculated by METIS and RISK.

4.4.1 Ionization

We decided to create the comparison of ionization profiles for separate beam energies of total NBI power (0.3 MW) for BBNBI and simplified ionization model. Third energy fraction ($E_0/3$) of beam composition was neglected due to its low abundance at these NBI powers. Ionization profiles has been calculated for electron density scan in range from $\approx 2.10^{19} m^{-3}$ to $\approx 8.10^{19} m^{-3}$. Ionization profiles calculated by BBNBI for energies $40keV$ and $20keV$ are shown in Fig. 4.10 and Fig. 4.11

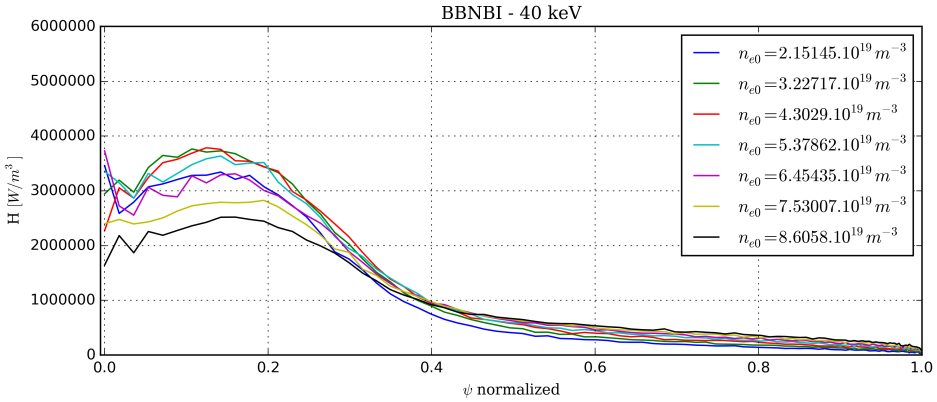

Figure 4.10: BBNBI - ionization profiles for the density scan ($40keV$)

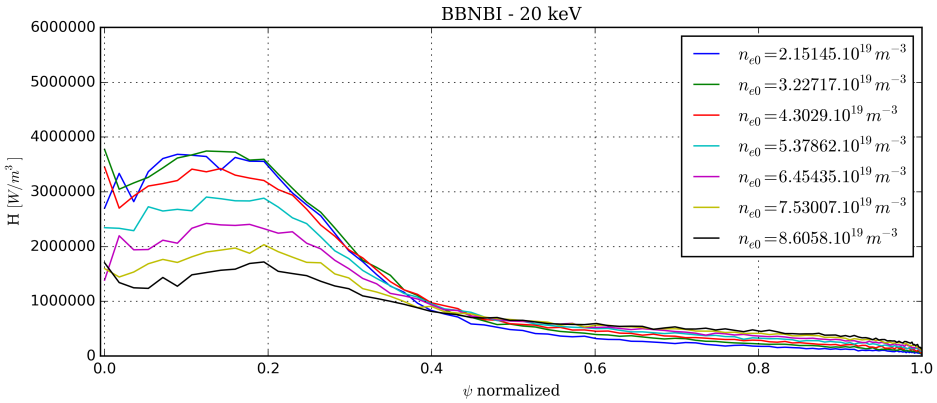

Figure 4.11: BBNBI - ionization profiles for the density scan ($20keV$)

The same electron density scan for energies $40keV$ and $20keV$ has been calculated by simplified ionization model. Results of this study is shown in Fig 4.12 and Fig 4.13.

We are going compare these models next to each other with ionization power densities and cumulative power integrated from the plasma center. Comparison of H profiles for BBNBI and simplified ionization model for energies $40keV$ and $20keV$ is shown in Fig. 4.14 and Fig.4.16. The same comparison for cumulative powers is shown in Fig. 4.15 and Fig.4.17.

As we can see, H profiles for both energies are pretty comparable. H-profile is almost the same from normalized ψ in the range from 0.4 to 1 in all cases and the main difference is in

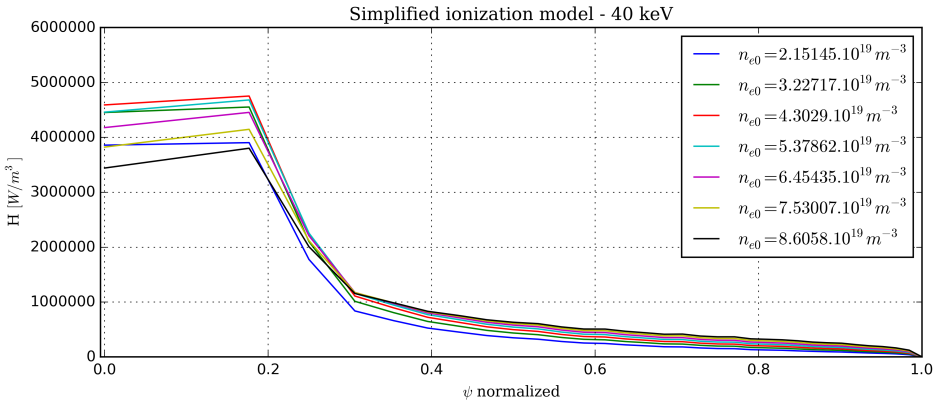

Figure 4.12: Simplified ionization model - ionization profiles for the density scan ($40keV$)

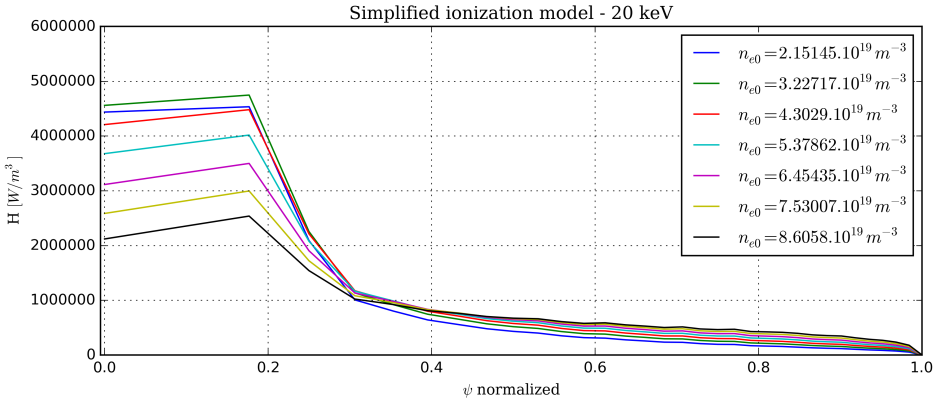

Figure 4.13: Simplified ionization model - ionization profiles for the density scan ($20keV$)

central plasma H profile. This difference is probably caused due to different approaches of beam ionization. While BBNBI is computing Monte Carlo simulation by following particular neutral atoms, the simplified model is calculating approximated linear differential equation. However, we are still getting pretty comparable results between both simulations.

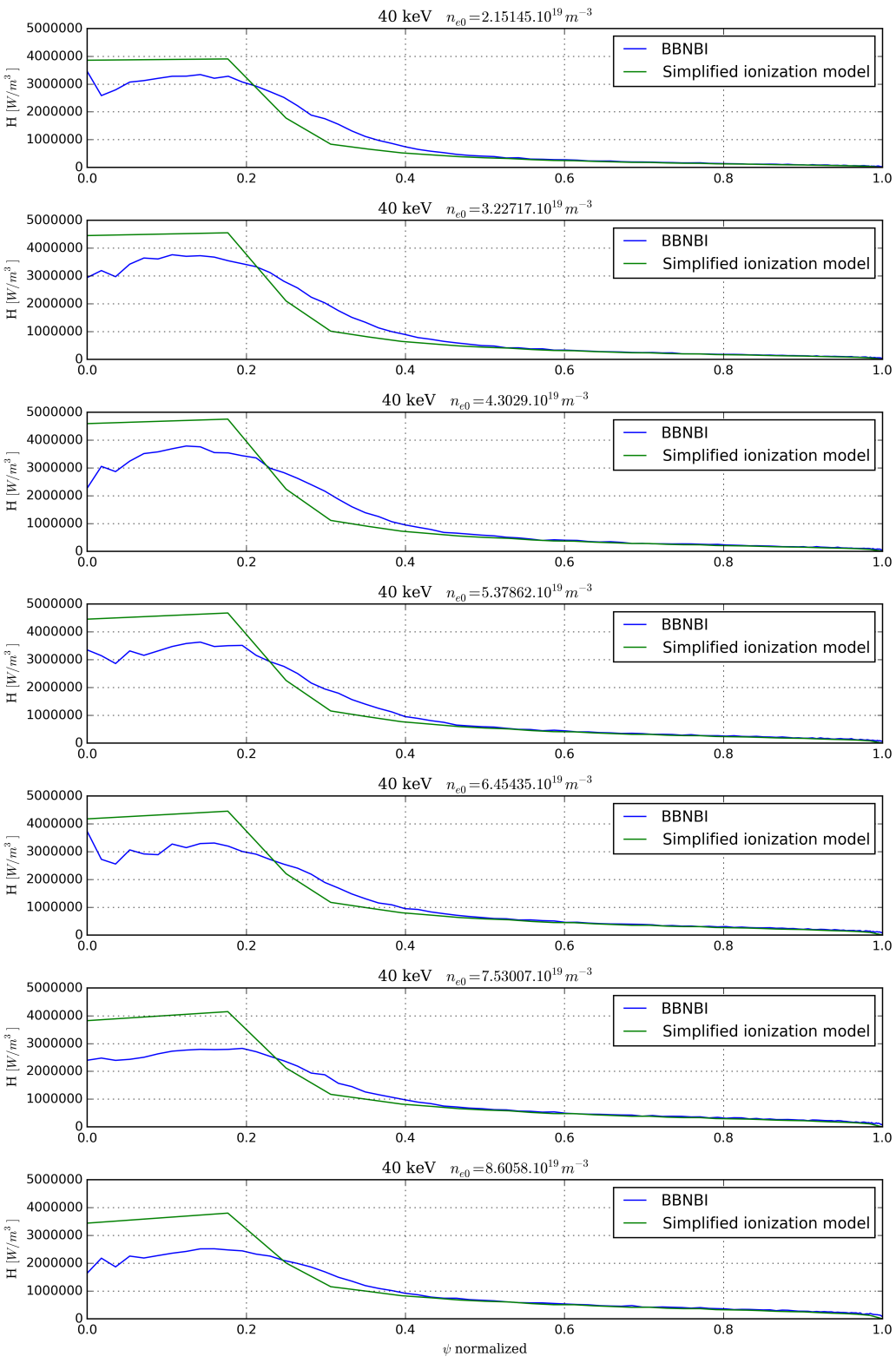

Figure 4.14: Comparison of BBNBI and Simplified model - H profile ($40keV$)

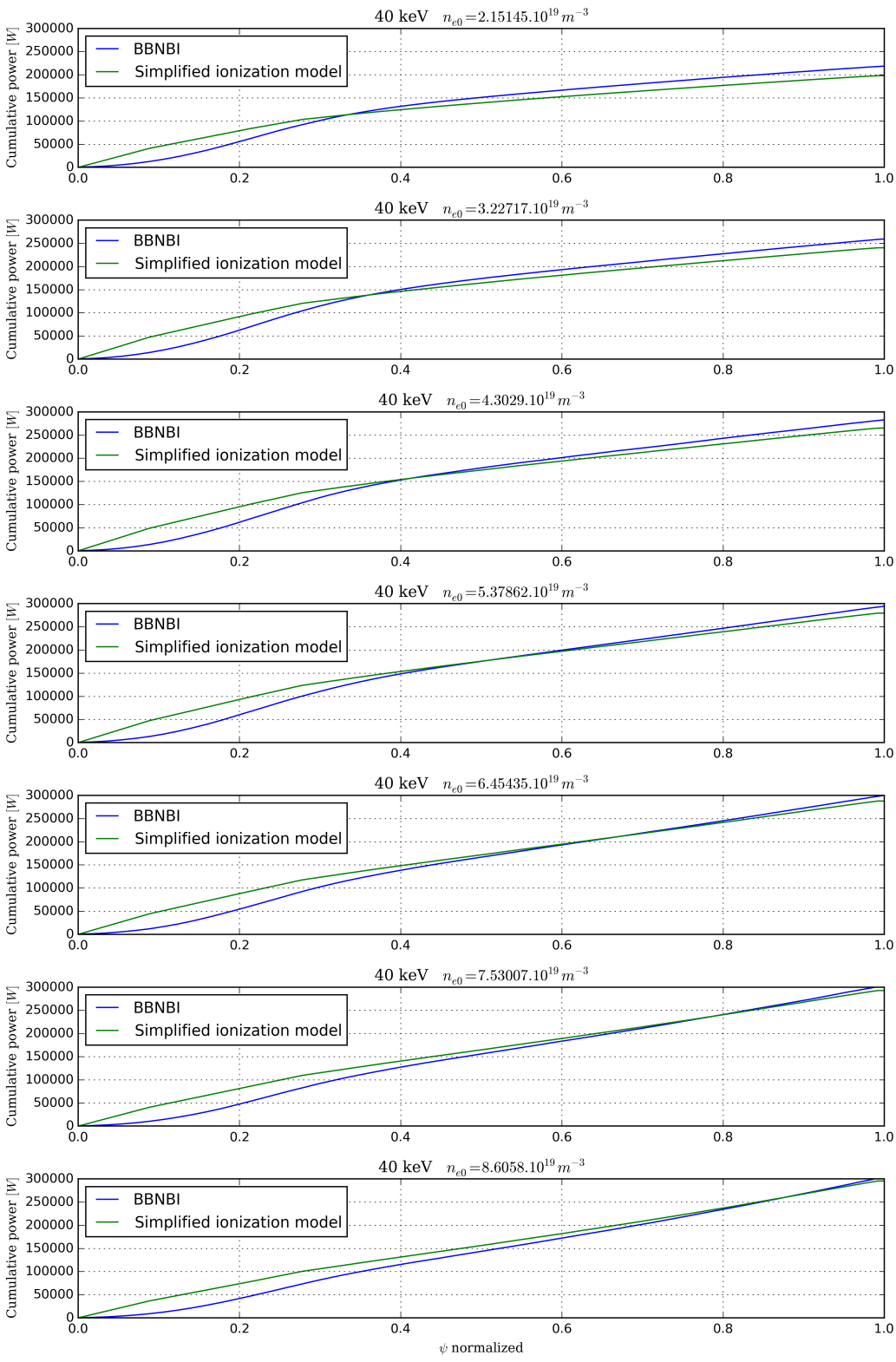

Figure 4.15: Comparison of BBNBI and Simplified model - Cumulative power ($40keV$)

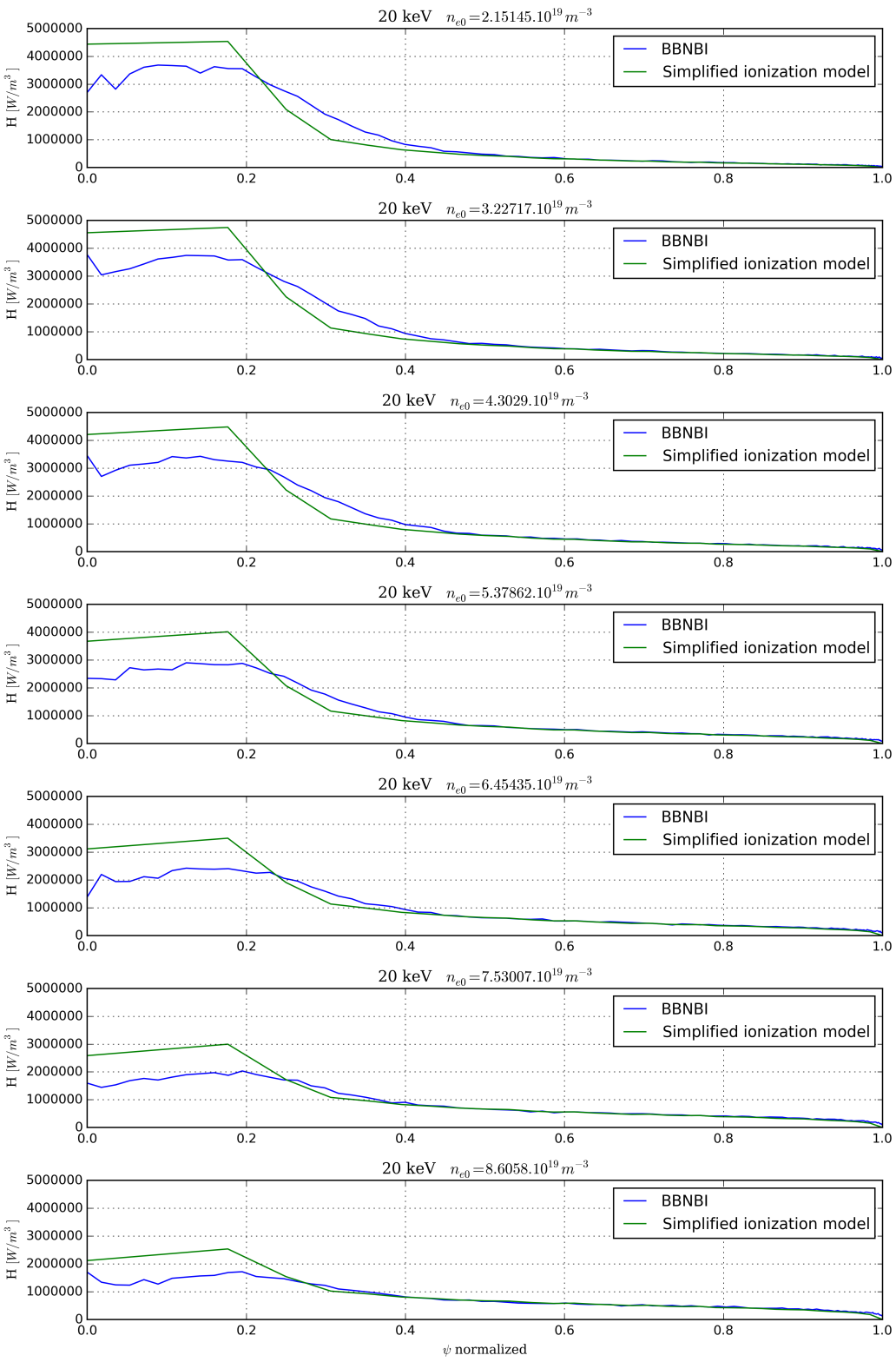

Figure 4.16: Comparison of BBNBI and Simplified model - H profile ($20keV$)

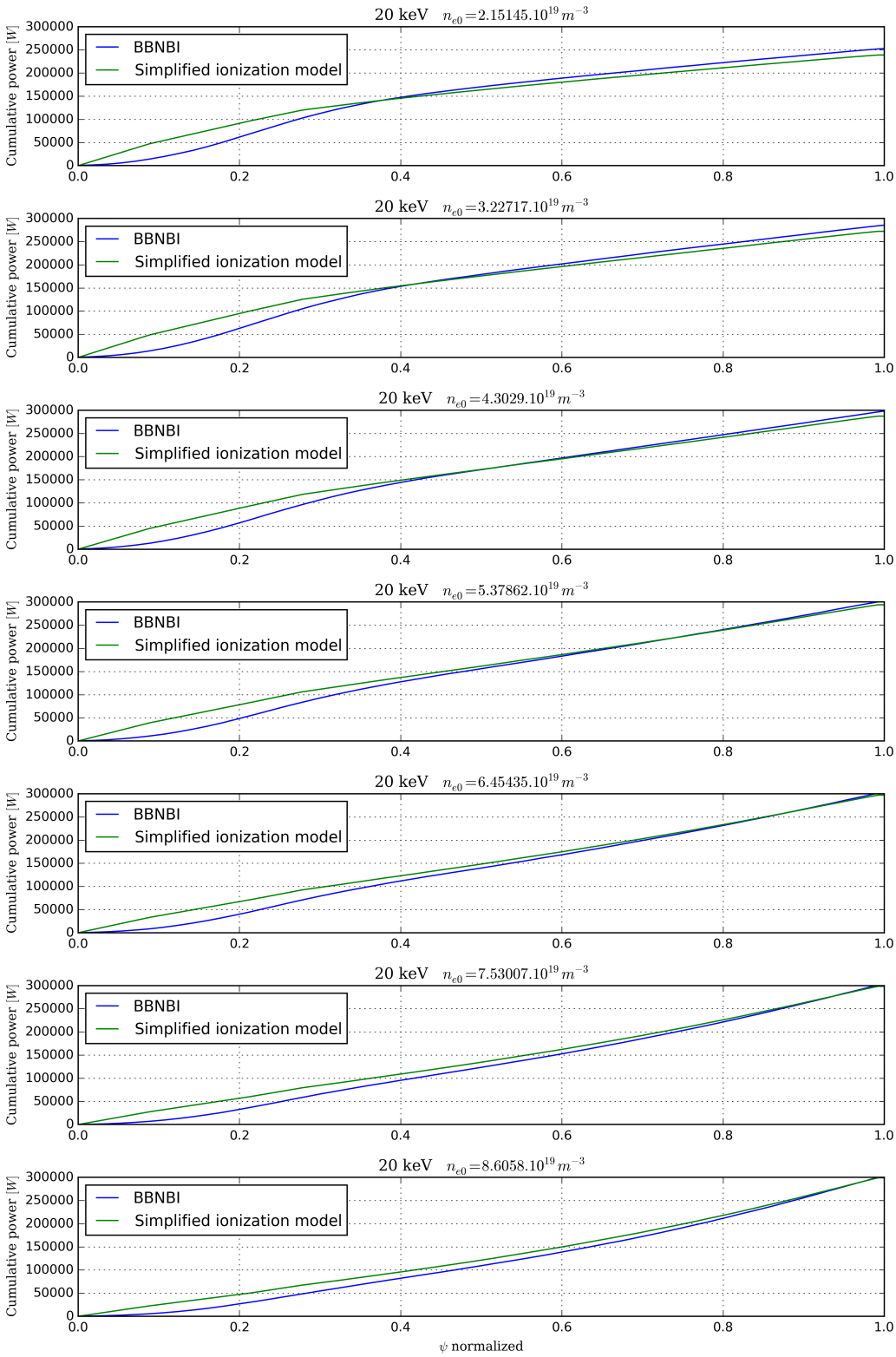

Figure 4.17: Comparison of BBNBI and Simplified model - Cumulative power ($20keV$)

We are getting another interesting result from profiles of cumulative ionized power, because of evaluation of shine through losses. Calculated shine through losses are shown in Table 4.1 and Table 4.2. Possible differences between the results could be caused by different ionization cross sections used in simulations.

Electron density	BBNBI	Simplified ionization model
$2.15 \times 10^{19} m^{-3}$	27.18%	34.02%
$3.22 \times 10^{19} m^{-3}$	13.55%	19.87%
$4.30 \times 10^{19} m^{-3}$	5.75%	11.63%
$5.38 \times 10^{19} m^{-3}$	1.94%	6.83%
$6.45 \times 10^{19} m^{-3}$	$\sim 1\%$	4.04%
$7.53 \times 10^{19} m^{-3}$	$\sim 1\%$	2.42%
$8.60 \times 10^{19} m^{-3}$	$\sim 1\%$	1.47%

Table 4.1: Shine through losses for BBNBI and Simplified ionization model ($40keV$)

Electron density	BBNBI	Simplified ionization model
$2.15 \times 10^{19} m^{-3}$	15.71%	20.38%
$3.22 \times 10^{19} m^{-3}$	4.85%	9.25%
$4.30 \times 10^{19} m^{-3}$	$\sim 1\%$	4.25%
$5.38 \times 10^{19} m^{-3}$	$\sim 1\%$	1.99%
$6.45 \times 10^{19} m^{-3}$	$\sim 1\%$	$\sim 1\%$
$7.53 \times 10^{19} m^{-3}$	$\sim 1\%$	$\sim 1\%$
$8.60 \times 10^{19} m^{-3}$	$\sim 1\%$	$\sim 1\%$

Table 4.2: Shine through losses for BBNBI and Simplified ionization model ($20keV$)

The largest value of shine through losses is approximately $15 - 30\%$ for densities in in range from $\sim 2 \times 10^{19}\mathrm{m}^{-3}$ to $\sim 3 \times 10^{19}\mathrm{m}^{-3}$. The result of this study shows us that shine through losses does not play a big role in the case of typical COMPASS tokamak plasma environment.

4.4.2 Beam thermalization

The beam thermalization has been simulated by RISK and METIS. We have decided to create the comparison of power density profiles (transferred to electron and ions) for separate beam energies ($E_0 = 40$keV and $E_0/2 = 20$keV) of total NBI power (0.3MW) for BBNBI and simplified ionization model. Third energy fraction ($E_0/3$) of the beam composition has been neglected for the same reason as in the case of ionization simulations. We have decided to create this comparison for higher electron density ($8.60 \times 10^{19}\mathrm{m}^{-3}$ to subtract the shine through effects and determine the effects of thermalization).

Comparison of the thermalization power density profiles and their cumulative powers for single 40keV energy component is shown in Fig. 4.18 and Fig.4.19 .

Fractions of total beam power (transferred to electrons and ions) for both energies are shown in Table 4.3 and table Table 4.4.

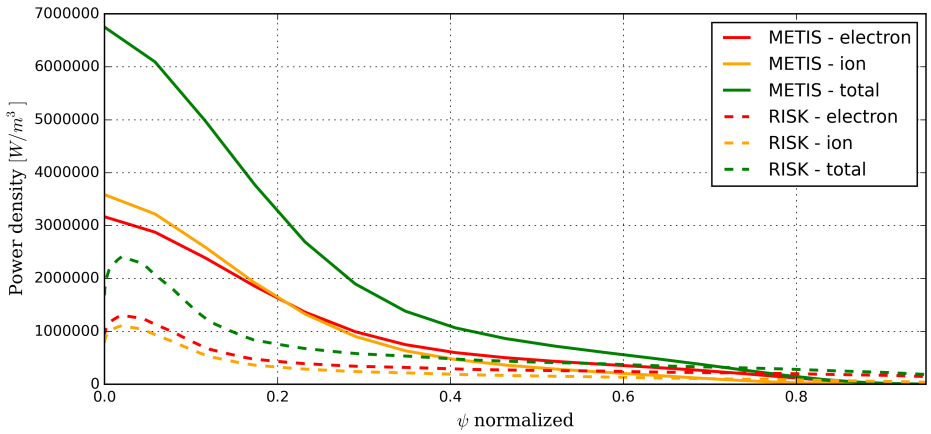

Figure 4.18: Comparison of RISK and METIS - Power density (40keV)

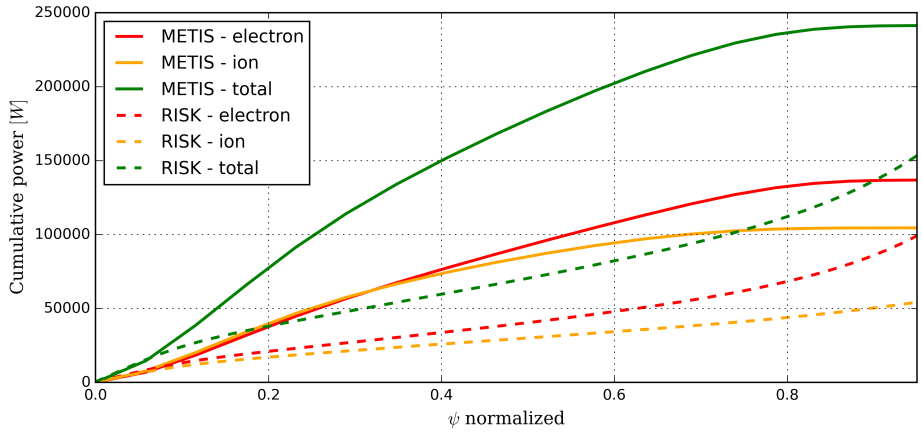

Figure 4.19: Comparison of RISK and METIS - Cumulative power (40keV)

40keV	RISK	METIS
Electrons	39.44%	45.60%
Ions	19.43%	34.82%

Table 4.3: NBI power transferred to electrons and ions calculated by RISK and METIS (40keV)

The same comparison of the thermalization power density profiles and their cumulative powers for single 20keV energy component is shown in Fig. 4.20 and Fig. 4.21 .

We can see the big difference between RISK and METIS thermalization calculation. This difference is observable for both energy components and both graphs of power densities and cumulative powers. The most probable cause of this difference is due to METIS simplified model of orbit losses calculation. We can see in the graphs of cumulative power (Fig. 4.19 and Fig. 4.21) that METIS profile at the plasma edge has derivative almost equal to zero. This effect is due to METIS assumption that fast ions generated nearby the plasma edge are

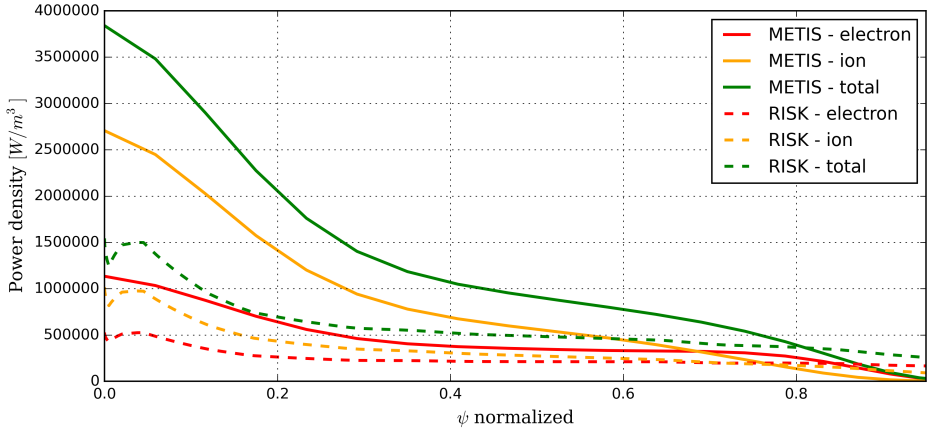

Figure 4.20: Comparison of RISK and METIS - Power density (20keV)

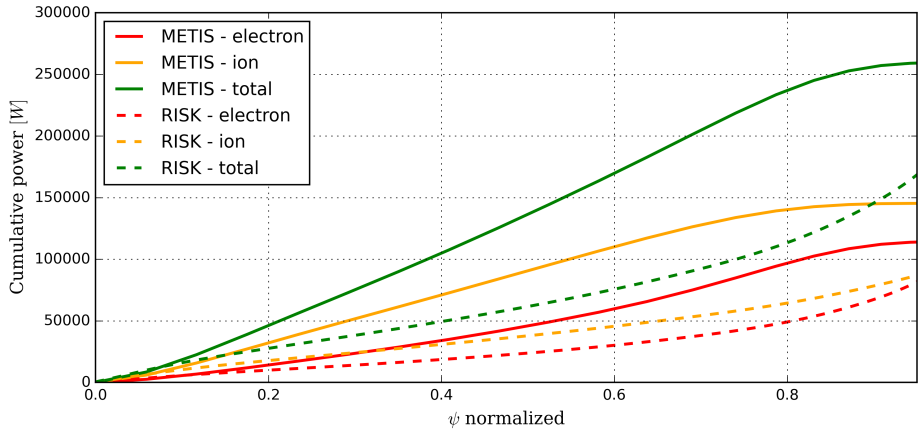

Figure 4.21: Comparison of RISK and METIS - Cumulative power ($20keV$)

$20keV$	RISK	METIS
Electrons	34.87%	38.08%
Ions	32.25%	48.42%

Table 4.4: NBI power transferred to electrons and ions calculated by RISK and METIS ($40keV$)

lost by orbit losses. This effect is not visible in functional dependency of RISK calculations because RISK calculates orbit losses by distributing source according to the fraction of time that ion stays at neighboring flux surfaces and derivative of this dependency nearby the plasma edge is positive. RISK calculations are much sophisticated and not that simplified as in the case of METIS simulations. METIS is using the scaling laws and simplified models to determine these quantities and this is the main reason why results of METIS calculations are much overrated than results of calculations by RISK. We need to take into our account all of these results and information for later comparison with experimental data.

Chapter 5

Experiments support by simulations

This chapter is going to be dedicated to the main topic of this thesis, support of experiments by simulations. In this chapter we are going to apply all of the information and knowledge acquired in previous chapters.

Support of experiments will be focused on NBI experiments of tokamak COMPASS. For this purpose we decided to choose experimental session that was intended for NBI. From this session we have chosen three tokamak discharges (shot numbers: 11031, 11033, 11034) of the electron density scan and high power of one NBI injector (0.3MW). High NBI power was chosen for high content of E_0 energetic beam component.

We used METIS and BBNBI with RISK to create simulations of NBI effects on tokamak discharges. It was mentioned in section (4.4.2) that METIS overrates NBI heating effects on plasma due to simplified assumption of beam absorption and scaling laws. We decided to compensate neglected METIS NBI losses by decreasing total input power of NBI (this assumption has not been taken into account in case of ITM simulations).

The experimental data are significantly limited due to the total count of diagnostic methods and their accompanied errors. We decided to create comparison of time dependent quantities as total energy content, electron and ion temperature and loop voltage between experimental data and data from METIS output. The input METIS data from experiment is the total plasma current, the averaged electron density and the plasma shape taken from EFIT.

After this procedure we have been repeatedly changing the input METIS parameters with an aim of satisfactory agreement between METIS data and data from experiment. The parameters, which we have been adjusting, were total input NBI power, H factor, ratio of electron and ion thermal conductivities and effective charge number. When we have noticed good agreement between METIS data and data from experiment, the METIS output data about NBI heating and current drive has been taken as relevant to discuss.

The input CPO data for BBNBI and RISK has been created for particular tokamak discharge (section 4.2). We have prescribed content of 80 percent for E_0 beam component and 20 percent for $E_0/2$ beam component. Third component $E_0/3$ has been neglected due to its low content and little affect on total absorbed power to plasma (Fig. 4.4). These parameters have been prescribed also in case of METIS simulations. Plasma profiles (electron and ion temperature and density, pressure, effective charge number ...) needed for BBNBI and RISK calculations have been taken from METIS output data at the beginning of NBI flat-top phase.

5.1 COMPASS tokamak discharge 11031

Discharge 11031 was one of "the middle value of electron density" discharges, therefore it was chosen as first for investigation by simulations. Basic discharge parameters during NBI are mentioned in Table 5.1.

Quantity	Value
Plasma current	193.21kA
Electron density	$5.48 \times 10^{19}\mathrm{m}^{-3}$
Magnetic field	1.15T

Table 5.1: Basic parameters of COMPASS tokamak discharge 11031

Total nominal NBI power has been calculated as product of total power accelerated ions before neutralizer and the neutralizer efficiency. Total NBI input power adjusted in METIS has been decreased to 63% of total power 0.3MW.

The scaling law used for METIS simulation is based on fitting the data from diamagnetic measurement of the total energy content. The effective charge number and H factor for METIS simulations have been set to time-indepent value 1. numb Experimental data for plasma energy content has been taken from EFIT and diamagnetic measurement [11, 27], electron temperature and density from Thomson scattering diagnostic [27], ion temperature from neutral particle analysis [28] and loop voltage from a flux loop [27]. A comparison of experiment and METIS is shown in Fig. 5.1.

Data for BBNBI and RISK has been taken from METIS output at the beginning NBI flat-top phase (1120ms) (Fig.5.1). Shine through losses calculated by simplified ionization model and BBNBI are in range from 1.5% to 3%. Result of calculated power densities transferred to electrons and ions and their cumulative powers are shown in Fig. 5.2. As we can see, there is visible difference between power transferred to electrons calculated by RISK and METIS. METIS makes an assumption that fast ions generated at the plasma edge are lost from the plasma volume by drift orbit losses. RISK calculates orbit losses by distributing source term described in section (4.2.2), therefore the ions generated at the plasma edge are not completely lost. Total power transferred to electrons and ions is shown in Table 5.2. The fraction of total NBI power calculated by METIS is a fraction of nominal NBI power 0.3MW, not the decreased one.

-	RISK	METIS
Electrons	55.92%	25.40%
Ions	19.29%	22.74%

Table 5.2: NBI power fractions calculated by RISK and METIS

Difference of these assumptions creates a difference between cumulative powers calculated by METIS and RISK. As we can see, RISK calculates that power deposited in the plasma edge is mostly transferred to electrons, due to low electron temperature and consequently low critical energy E_c. The relevant information about power transferred to electrons should

be some compromise between METIS and RISK. Profiles of power density and cumulative power transferred to ions show us comparable results in both cases (RISK, METIS), therefore the results of power transferred to ions could be taken as relevant. Comparable results of ion power density profiles lead us to reconstruction of ion distribution functions for parallel velocity Fig. 5.3.

5.2 COMPASS tokamak discharge 11033

Discharge 11033 was chosen for its high value of electron density. Basic discharge parameters during NBI are mentioned in Table 5.3.

Quantity	Value
Plasma current	196.77kA
Electron density	$8.87 \times 10^{19}\mathrm{m}^{-3}$
Magnetic field	1.15T

Table 5.3: Basic parameters of COMPASS tokamak discharge 11033

Result of data agreement between experiment and METIS is shown in Fig. 5.4. Total NBI input power adjusted in METIS has been decreases to 57% of total power $0.3MW$. Experimental data for plasma energy content, electron and ion temperature and loop voltage has been taken the same way as in case of discharge number 11031. The scaling law used for METIS simulation is based on fitting the data from diamagnetic measurement of the total energy content. The effective charge number and H factor for METIS simulations have been set to time-indepent values $Z_{eff} = 1.1$ and $H = 1$.

Shine through losses calculated by simplified ionization model and BBNBI are very low ($\sim$ 1%), due to high electron density. Result of calculated power densities transferred to electrons and ions and their cumulative powers are shown in Fig. 5.5.

Firstly we can see the differences functional dependencies between METIS and RISK. This effect probably comes from calculation of ionization profile H. Differences in calculations of ionization cross-section are the most probable cause of different functional dependences of power density. Total power transferred to electrons and ions is shown in Table 5.4. The effect of plasma edge electron heating is recognizable at the same rate as in case of discharge 11031 in previous section. However cumulative power of power transferred to ions reaches almost the same result in case of both simulations (METIS, RISK). The fraction of total NBI power calculated by METIS is a fraction of nominal NBI power 0.3MW, not the decreased one.

-	RISK	METIS
Electrons	63.56%	24.36%
Ions	16.38%	16.03%

Table 5.4: NBI power fractions calculated by RISK and METIS

Due to satisfactory comparison of power density and cumulative power transferred to ions, we decided to reconstruct profile of ion distribution function. Profile of ion distribution

function is shown in Fig. 5.6. We can see in Fig 5.6 slight shift of the distribution function maximum to the higher parallel velocities, this effect corresponds to the total plasma heating. The same effect is visible in case of discharge 11031.

5.3 COMPASS tokamak discharge 11034

Discharge 11034 was chosen for its low value of electron density. Basic discharge parameters during NBI are mentioned in Table 5.5.

Quantity	Value
Plasma current	198.87 kA
Electron density	$3.25 \times 10^{19}\mathrm{m}^{-3}$
Magnetic field	1.15 T

Table 5.5: Basic parameters of COMPASS tokamak discharge 11034

Result of data agreement between experiment and METIS is shown in Fig. 5.7. Total NBI input power adjusted in METIS has been decreases to 43% of total power $0.3MW$. Experimental data for plasma energy content, electron and ion temperature and loop voltage has been taken the same way as in case of discharge number 11031. The effective charge number and H factor for METIS simulations have been set to time-indepent values $Z_{eff} = 2$ and $H = 1$. The scaling law used for METIS simulation is based on standard ITER scaling law [26]. Shine through losses calculated by simplified ionization model and BBNBI are approximately $\sim$ 15%, due to low electron density. Result of calculated power densities transferred to electrons and ions and their cumulative powers are shown in Fig. 5.8. As we can see in the figure of power density (Fig. 5.8), neutral beam is mostly heating the plasma center. This effect is due to profile of electron density because the beam has been ionized mostly in the region of higher electron density, the plasma center. Comparable results of the total power transferred to the electron and ions calculated by RISK and METIS is shown in Table 5.6. The fraction of total NBI power calculated by METIS is a fraction of nominal NBI power 0.3MW, not the decreased one.

-	RISK	METIS
Electrons	25.25%	16.14%
Ions	21.25%	19.98%

Table 5.6: NBI power fractions calculated by RISK and METIS

The ion distribution function has been calculated by RISK (5.9). We can see in the tail of ion distribution function two "steps" corresponding to beam composition fractions ($40keV$ and $20keV$). This effect is most recognizable at the lower densities because the beam fast particle contribution is the most expressive at these plasma densities. This effect is also recognizable in case of ion distribution function of discharge 11031. The beam fast particle contribution was the least recognizable in the case of discharge 11033 because of its high plasma density.

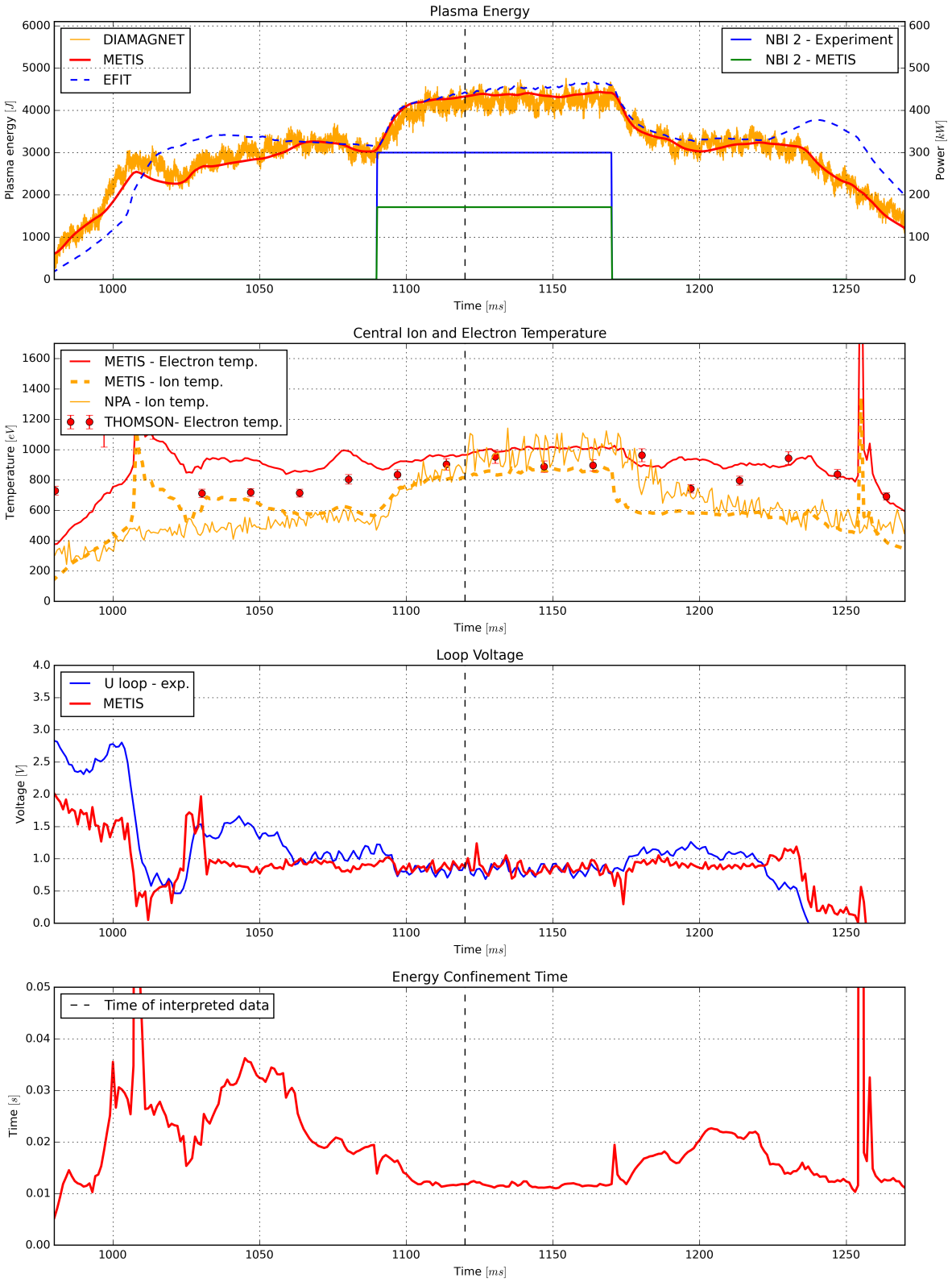

Figure 5.1: Comparison of experiment and METIS (discharge 11031)

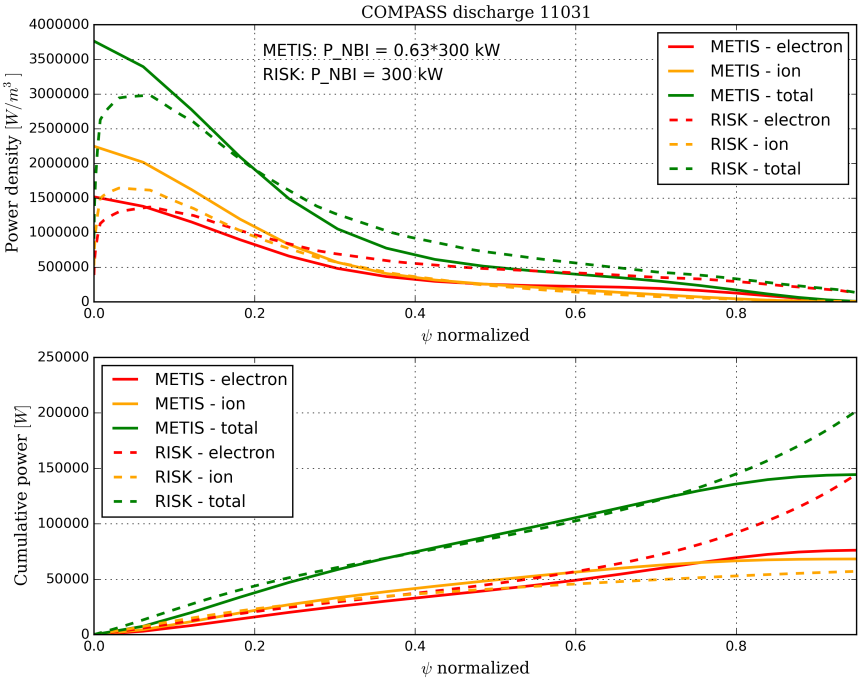

Figure 5.2: Power density and cumulative power transferred to electrons and ions (discharge 11031)

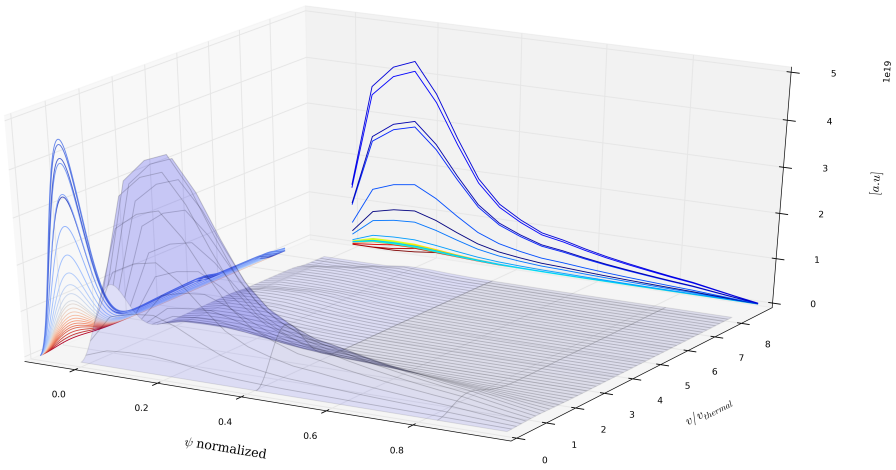

Figure 5.3: Profiles of ion distribution function calculated by RISK (discharge 11031)

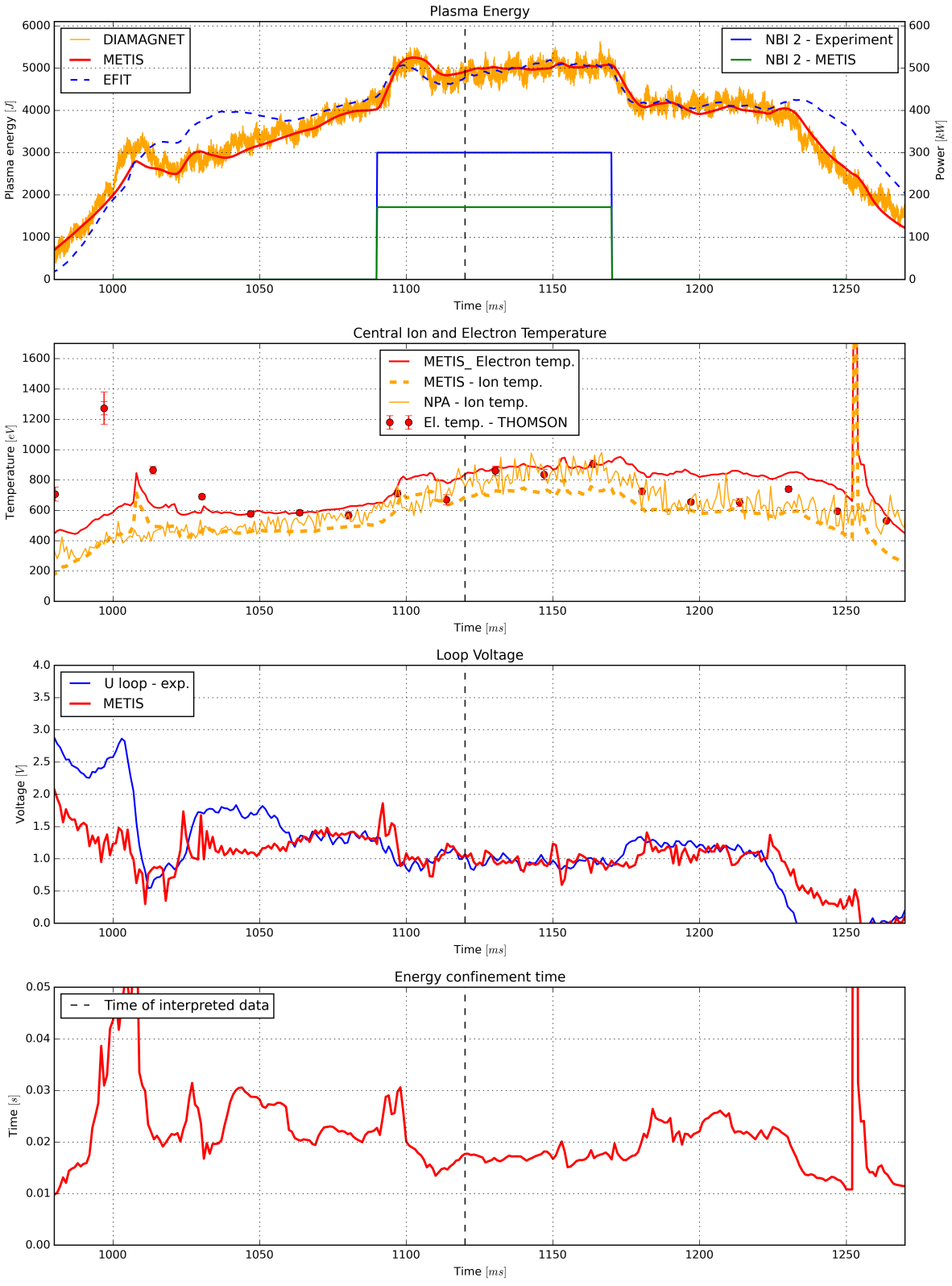

Figure 5.4: Comparison of experiment and METIS (discharge 11033)

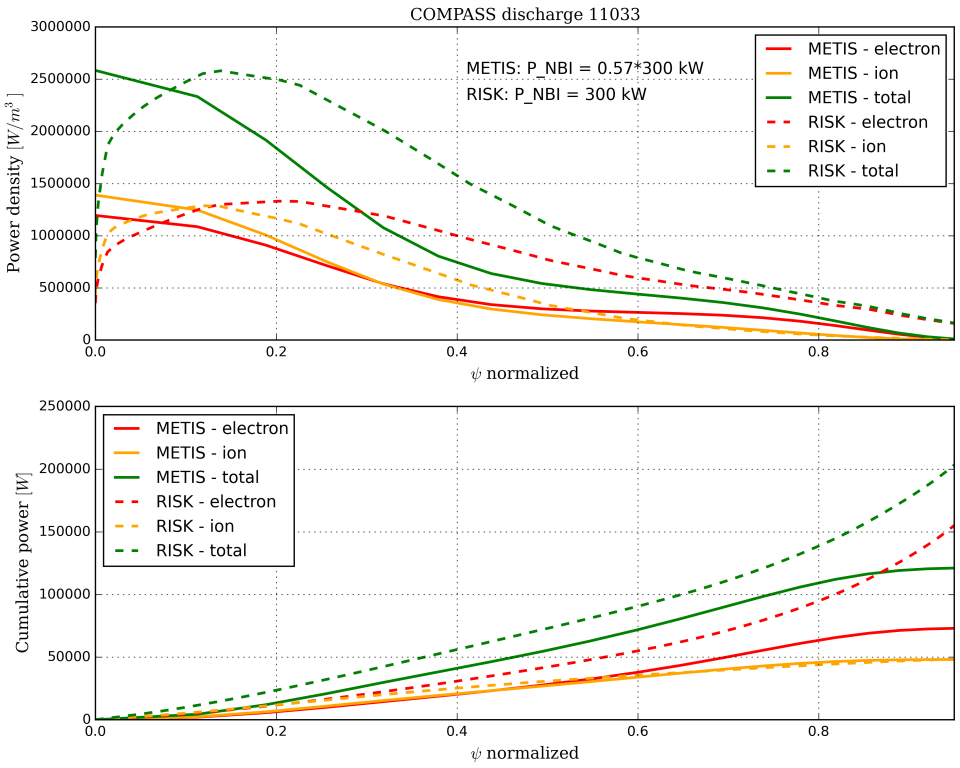

Figure 5.5: Power density and cumulative power transferred to electrons and ions (discharge 11033)

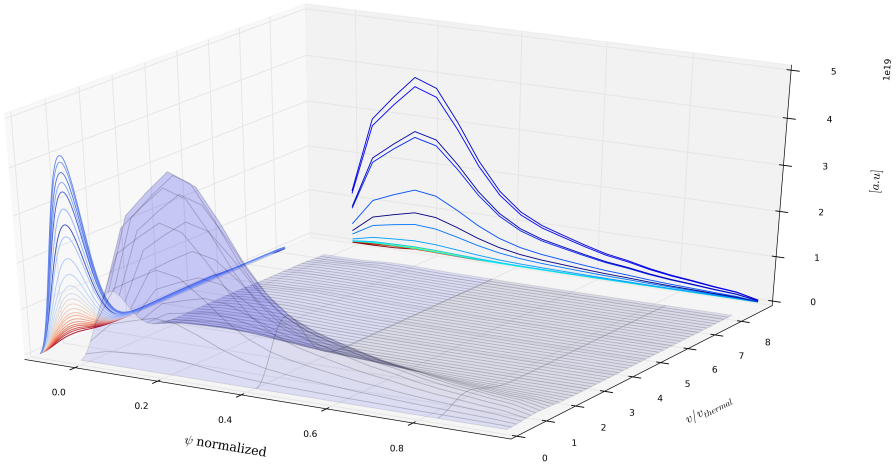

Figure 5.6: Profiles of ion distribution function calculated by RISK (discharge 11033)

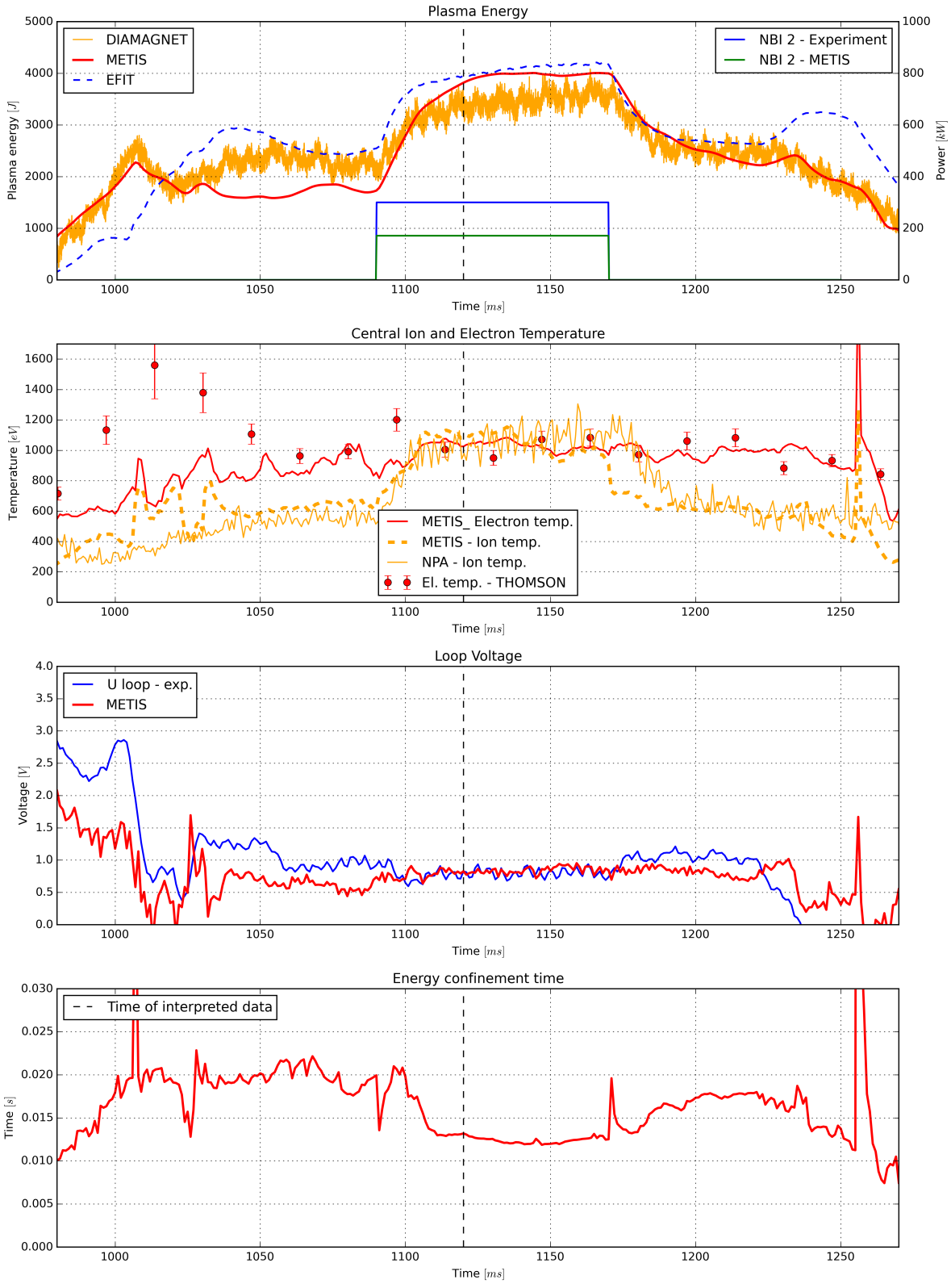

Figure 5.7: Agreement between experiment and METIS (discharge 11034)

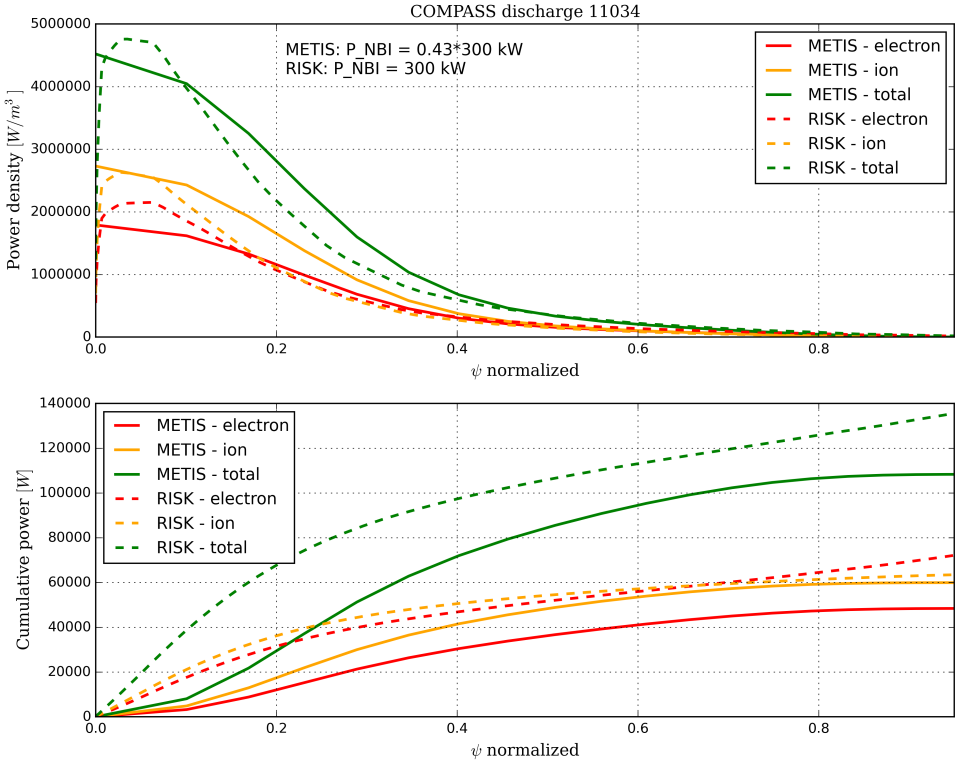

Figure 5.8: Power density and cumulative power transferred to electrons and ions (discharge 11034)

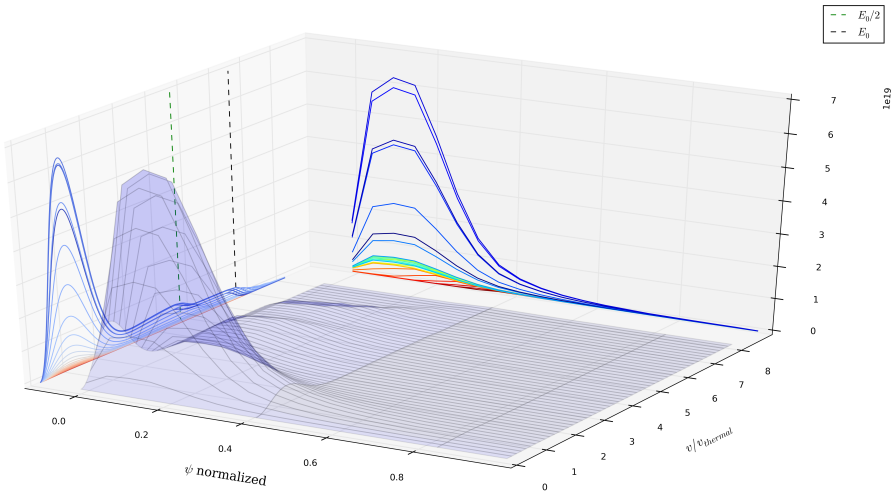

Figure 5.9: Profiles of ion distribution function calculated by RISK (discharge 11034)

Chapter 6

Summary

COMPASS tokamak experiments support by simulations was the main topic of this thesis. For successful acquaintance with this topic, it was necessarily needed to acquire knowledge about thermonuclear fusion and magnetically confined plasma.

The first chapter was dedicated to basic physical and technological background of controlled thermonuclear fusion. We realized that the state of matter at temperatures needed to fuse hydrogen nuclei is called high-temperature plasma. The temperature of this state of matter is so high that the only possible way to contain this matter is by use of appropriate configuration of electromagnetic fields. One of the reactors that create mentioned appropriate magnetic field configuration is called tokamak, the most successful approach to controlled thermonuclear fusion.

Every thermonuclear reactor and also tokamak has to be equipped by a certain method of plasma heating to achieve those thermonuclear temperatures. The first known method of plasma heating mechanism was Ohmic heating, but unfortunately this heating method becomes ineffective to heat plasma to thermonuclear temperatures. Therefore was needed another heating method which would be sufficient to cover this gap.

Successful approach to heat the plasma to thermonuclear temperatures is called neutral beam injection - NBI. This heating method was discussed in the second chapter of this thesis. NBI is based on injection of high energetic neutral atoms inside the thermonuclear reactor. The neutral atoms are ionized by particular ionizations processes and then the created fast ions transfer their kinetic energy to plasma particles by Coulomb collisions. The resultant effect is an increase in the plasma temperature.

The second chapter discussed particular physical processes of neutral beam ionization, trajectories of the ionized injected atoms and the resultant fast ion thermalization inside the tokamak plasma. Another discussed topic of this chapter is the technological aspect of the neutral beam creation including the description of the ion source, the acceleration of generated ions and the neutralization of the accelerated ions.

Effects of NBI in tokamak plasmas are difficult to determine in general by simple mathematical derivations, but computer simulations are an apparatus which is able to determine these physical effects very effectively. Simulations are able to verify consistency of experimental data from diagnostic systems, or even additionally calculate quantities, which are not directly measured. The third chapter was dedicated to numerical simulation models and

their comparisons focused on simulations of NBI in tokamaks. The simulations and their comparisons have been made on discharges of tokamak COMPASS plasma environment.

One of the points of this thesis was the development of a simple ionization model of NBI applied for plasma discharges on tokamak COMPASS. The principle of this simplified ionization model is based on solving the equation of the neutral beam attenuation by ionization processes inside the COMPASS tokamak plasma. Solving the equation required definition of the neutral beam geometry, the profile of electron density along the beam trajectory and the ionization cross sections of particular ionization processes. Motivation for development of this model was to determine the ionization power profiles (denoted by H) and so-called shine through losses when the neutral beam is not sufficiently attenuated inside the tokamak plasma. The result of this study has shown that for typical tokamak COMPASS environment the shine through losses are in range of a few percent and does not play a big role.

The NBI simulations of tokamak COMPASS discharges have been also made by sophisticated models from the EUROfusion integrated modelling effort (EU-IM). BBNBI (Beamlet Based NBI) code was used for Monte Carlo computation of beam ionization and RISK (Rapid Ion Solver for toKamaks) code for simulating the evolution of the distribution function of NBI plasmas. BBNBI calculation of the beam ionization creates an ensemble of fast test ions assigned to RISK distribution function calculation.

We needed to create input data structure for these simulation codes. Data structure for these codes is so called CPO (Consistent Physical Object). The CPO-s for our purposes had to contain information about neutral beam injector parameters, tokamak vessel, profiles of plasma quantities and magnetohydrodynamic equilibrium calculated by Grad-Shafranov equation.

The comparison of the BBNBI and simplified ionization model has shown comparable results between these two simulations. Possible differences were probably caused due to different approaches of beam ionization. While BBNBI is computing Monte Carlo simulation by following particular neutral atoms, the simplified model is calculating approximated linear differential equation. Another possible difference was probably caused by different ionization cross sections used in both simulations. BBNBI proved that shine through losses do not play a great role in the typical tokamak COMPASS environment.

The beam thermalization has been simulated by RISK and METIS. The METIS (Minute Embedded Tokamak Integrated Simulator) code has been developed to simulate tokamak plasma temporal evolution using information from scaling laws chained with simplified source models and using an almost always convergent computing scheme that enables to simulate a full plasma discharge in a time of approximately one minute.

The comparison between RISK and METIS has been made for higher electron density tokamak discharge to subtract the shine through effects and determine the effects of thermalization. The big difference has been noticed between RISK and METIS thermalization calculation. METIS calculation has shown significantly more effective power deposition (i.e.

lower losses) in comparison with RISK. The most probable cause of this difference is due to METIS simplified model of orbit losses (when injected ions are lost from tokamak plasma volume while traveling along the trajectories determined by the tokamak magnetic field configuration) calculation. RISK calculates orbit losses by distributing source according to the fraction of time that ion stays at neighboring flux surfaces (surfaces of constant magnetic flux). METIS is using the scaling laws and simplified models to determine these quantities and this is the main reason why the results of METIS calculations are much overrated compared to results of calculations by RISK.

Reasonable compensation of simplified METIS calculation of NBI losses was made by decreasing the total input power of NBI, with an aim of simulating loss processes of certain kind. This assumption has not been taken into account in case of RISK simulations.

The last chapter was dedicated to experiments support by simulations. The support of experiments has been focused on NBI experiments of tokamak COMPASS. It has been chosen experimental session that was intended for NBI. From this session has been chosen three tokamak discharges (shot numbers: 11031, 11033, 11034) of the electron density scan and high power of one NBI injector (0.3MW).

I have made a comparison of time dependent quantities between experimental data and data from METIS simulations. In this procedure, the input METIS parameters have been repeatedly changed with the aim of satisfactory agreement with the data from the experiment. When there has been noticed good agreement between the data, the METIS output data about NBI heating has been taken as relevant to discuss.

COMPASS tokamak discharge 11031 was one of the middle value of electron density discharges. Total NBI input power adjusted in METIS has been decreased to 63% of the nominal NBI power used in experiment. With the assumption that 37% of NBI power has been lost, a satisfactory agreement between the METIS simulation and the experiment is found. After this procedure, the input data for BBNBI and RISK have been taken from METIS output at the beginning of NBI flat-top phase. The shine through losses calculated by simplified ionization model and BBNBI were in range from 1.5% to 3%, which is not a significant NBI power loss. RISK calculation has shown that the fraction of the total power transferred electrons is approximately 56% percent and the METIS calculation has shown 25% (this is a fraction of total nominal NBI power 0.3MW, not the decreased one). RISK has calculated that the power deposited in the plasma edge is mostly transferred to electrons, which has not been noticed by METIS calculations. The difference of these numbers is probably due to different assumptions of NBI power deposition. The relevant information about power transferred to electrons should be some compromise between METIS and RISK. The profiles of NBI power transferred to ions has shown comparable results in case of both simulations (RISK: 19%, METIS: 23%), therefore the results of power transferred to ions could be taken as relevant.

The second COMPASS tokamak discharge chosen for investigation by simulations was discharge 11033. This discharge was chosen for its high electron density. Total NBI input

power adjusted in METIS has been decreased to 57% of the nominal NBI power used in experiment. The procedure of creation the input and output data has been the same as in case of discharge number 11031. Shine through losses calculated by the simplified ionization model and BBNBI were less than 1%, which is almost negligible. The effect of plasma edge electron heating is recognizable at the same rate as in case of discharge 11031 (RISK: 64%, METIS: 24%), but total the power transferred to ions reaches almost the same result in case of both simulations: 16%.

The last COMPASS tokamak discharge chosen for investigation by simulations was discharge 11034. This discharge was chosen for its low electron density. Total NBI input power adjusted in METIS has been decreased to 43% of the nominal NBI power used in experiment. The procedure of creation the input and output data has been the same as in case of discharges 11031 and 11033. Shine through losses calculated by simplified ionization model and BBNBI were approximately 15%, which was the effect of low electron density. This discharge has also noticed the highest orbit losses calculated by RISK (39%).

Simulations by RISK and METIS have shown comparable results after decrease of input NBI power used by METIS. The decrease of the input NBI power used by METIS could be explained as compensation of power losses that are underrated (orbit losses) or not assumed by METIS. The possible explanations that NBI power is not absorbed in the plasma (besides the simplified assumptions) are that the efficiency of the NBI neutralizer is worse than expected or the neutral beam injector is blocked with working gas due to ineffective vacuum pumping neutral beam injector ("NBI blocking").

The biggest difference between the simulations has been noticed at NBI power transferred to electrons at the plasma edge. This difference has origin in different calculation of orbit losses by both simulation models. The relevant information about the power transferred to electrons should be some compromise between METIS and RISK. Profiles of NBI power transferred to ions have shown comparable results in case of both simulations. This result has been the main reason to reconstruct the profiles of ion distribution function. The effect of total plasma heating and an increase in population of fast ions in the plasma were shown on the profiles of the distribution function.

This study has shown that we are able simulate quantities as ionized power profiles, NBI power transferred to electrons and ions and the ion distribution functions for COMPASS tokamak discharges by using numerical simulations. These results are valuable because the mentioned quantities are not directly measured by plasma diagnostics. The results of this thesis can be further enhanced and verified by particle following Monte Carlo codes.

The numerical simulations are not pertained just to tokamak COMPASS experiments. We owe numerical simulations for progress in general and therefore they take inseparable place in scientific world.

Bibliography

[1] Wesson, J. and D.J. Campbell, *Tokamaks*, Oxford University Press, New York,(2004).

[2] S. Atzeni,J. Meyer-ter-Vehn, *The Physics of Inertial Fusion: Beam Plasma Interaction, Hydrodynamics, Hot Dense Matter*, Oxford Univ. Press, Oxforf (2004).

[3] Freidberg, J. P., *Plasma physics and fusion energy* (2007).

[4] V.Martisovitš. *High-temperature plasma 1,2*, Lectures, FMFI UK Bratislava,(2013/2014).

[5] K. Lackner, et al, *Fusion Physics*, International Atomic Energy Agency, Vienna,(2012)

[6] Kulhánek P., *Uvod do teorie plazmatu*, AGA, Prague, (2011).

[7] R.Fitzpatrick, *Magnetic Mirrors*, Home Page for Richard Fitzpatrick, The University of Texas at Austin, (2011).

[8] F.F. Chen, *Úvod do fyziky plazmatu*, Praha: Academia (1984).

[9] Spitzer L. et al., *The Stellarator Concept*, The Physics of Fluids, 1 (4): 253, doi:10.1063/1.1705883,(1958).

[10] EUROfusion reference: *https://www.euro-fusion.org/wpcms/wp-content/uploads/2011/07/7c.jpg*

[11] J. Havlicek J. Urban, *A Magnetic Equilibrium Reconstruction in Tokamak*, WDS07 Proceedings of Contributed Papers, Part II, 234–239,ISBN 978-80-7378-024-1,(2007).

[12] EUROfusion reference: *https://www.euro-fusion.org/2011/09/tokamak-principle-2/*

[13] Doyle, E.J., et al., *ITER physics basis*, Nuclear Fusion, (2007).

[14] MAZZUCATO E., *Electromagnetic Waves for Thermonuclear Fusion Research*, Singapore: World Scientific, ISBN 9789814571807, (2014).

[15] Speth, E., *Neutral Beam Heating of Fusion Plasmas*, Reports on Progress in Physics, 52(1): p. 57-121 (1989).

[16] Kikuchi, Lackner, Tran. *Fusion Physics*, IAEA,p.539,(2012).

[17] Urban, J., et al., *Self-consistent transport simulations of COMPASS operation with optimized NBI*, Plasma Physics and Controlled Fusion, 52(4): p. 045008 (2010)

[18] R. Koch, *Fast particle heating*, Laboratory for Plasma Physics, Ecole Royale Militaire -Koninklijke Militaire SchoolB-1000 Brussels, Belgium (2012).

[19] Jardin, S., *Computational methods in plasma physics*, (2010).

[20] *ITER TECHNICAL BASIS*, IAEA, Vienna, (2002).

[21] R.Pánek et al., *Reinstallation of the COMPASS-D Tokamak in IPP ACSR.*, Czechoslovak Journal of Physics, 56(2):B125-B13, (2006).

[22] Urban, J., et al., *NBI system for reinstalled COMPASS-D tokamak.*, Czechoslovak Journalof Physics, 56(Suppl. B): p. B176-B181 (2006).

[23] EU-IM reference: *http://www.euro-fusionscipub.org/eu-im*

[24] Asunta O. et al., *Modelling neutral beams in fusion devices: Beamlet-based model for fast particle simulations*, Computer Physics Communications, 188, 33-46 (2015).

[25] M. Schneider et al., *A rapid fast ion Fokker–Planck solver for integrated modelling of tokamaks*, Nuclear Fusion 55, 013003 (12pp), (2014).

[26] Artaud J.F., *METIS User's Guide*, Institute for Magnetic Fusion Research, France,(2008).

[27] I. H. Hutchinson, *Principles of Plasma Diagnostics*, Cambridge University Press, Cambridge, (2002).

[28] IOFFE PHYSICAL-TECHNICAL INSTITUTE OF THE RUSSIAN ACADEMY OF SCIENCES, *Multichannel Neutral Particle Analyzer ACORD-24: Instructions and Operating Manual*, St. Petersburg,(2011).